

Forecasting temporal variation of aftershocks immediately after a main shock using Gaussian process regression

Kosuke Morikawa¹, Hiromichi Nagao^{2,3}, Shin-ichi Ito^{2,3}, Yoshikazu Terada^{1,4}, Shin'ichi Sakai^{2,5} and Naoshi Hirata^{2,6}.

¹ Graduate School of Engineering Science, Osaka University, 1-3, Machikaneyama-cho, Toyonaka-shi, Osaka 560-8531, Japan.

² Earthquake Research Institute, The University of Tokyo, 1-1-1, Yayoi, Bunkyo-ku, Tokyo 113-0032, Japan.

³ Graduate School of Information Science and Technology, The University of Tokyo, 7-3-1, Hongo, Bunkyo-ku, Tokyo 113-8656, Japan.

⁴ Center for Advanced Intelligence Project, RIKEN, 1-4-1, Nihonbashi, Chuo-ku, Tokyo 103-0027, Japan.

⁵ Interfaculty Initiative in Information Studies, The University of Tokyo, 7-3-1, Hongo, Bunkyo-ku, Tokyo 113-0033, Japan.

⁶ National Research Institute for Earth Science and Disaster Resilience, 3-1, Tennodai, Tsukuba-shi, Ibaraki 305-0006, Japan.

SUMMARY

Uncovering the distribution of magnitudes and arrival times of aftershocks is a key to comprehending the characteristics of earthquake sequences, which enables us to predict seismic activities and conduct hazard assessments. However, identifying the number of aftershocks immediately after the main shock is practically difficult due to contaminations of arriving seismic waves. To overcome this difficulty, we construct a likelihood based on the detected data, incorporating a detection function to which Gaussian process

regression (GPR) is applied. The GPR is capable of estimating not only the parameters of the distribution of aftershocks together with the detection function, but also credible intervals for both the parameters and the detection function. The property that the distributions of both the Gaussian process and aftershocks are exponential functions leads to an efficient Bayesian computational algorithm to estimate hyperparameters. After its validation through numerical tests, the proposed method is retrospectively applied to the catalog data related to the 2004 Chuetsu earthquake for the early forecasting of the aftershocks. The results show that the proposed method stably and simultaneously estimates distribution parameters and credible intervals, even within $t \leq 3\text{h}$ after the main shock.

Key words: Statistical seismology; Statistical methods; Probability distributions; Probabilistic forecasting; Time series analysis.

1 INTRODUCTION

A massive earthquake triggers a number of aftershocks. The classical representative models to describe the temporal distribution of aftershocks were established as the Omori-Utsu (Omori 1894; Utsu 1961) and the Gutenberg-Richter (Gutenberg & Richter 1944) formulae, the latter of which also considers information on magnitudes. Ogata (1988) proposed, having extended the Omori-Utsu formula, the Epidemic Type Aftershock Sequence (ETAS) model to describe more realistically that large aftershocks also excite subsequent aftershocks, similar to the main shock. The distribution of aftershocks enables forecasting seismic activities and conducting hazard assessments (Resenberg & Jones 1989, 1994; Kagan & Jackson 2000). Until now, previous studies have proposed many statistical methods to estimate the parameters involved in the models (Aki 1965; Ogata 1983, 1988). A disadvantage of these parameter estimation methods is that they assume the existence of a complete dataset without missing values. However, detecting all aftershocks immediately after the main shock is unrealistic due to contaminations by a tremendous amount of seismic waves. Such incomplete data cause underestimations in the counting of aftershocks at the time-dependent completeness magnitude.

In statistics, situations in which only some detected data are available are known as biased sampling problems (Vardi 1982, 1985). In our case, the detection probability of aftershocks clearly depends on the magnitudes and elapsed time from the main shock. This type of biased sampling data is termed as “missing not at random” (MNAR), in which the detection probability depends on the values of undetected data. Introducing a detection function, which is a model of the detection probability,

enables correcting the bias (Qin 2017). Several studies have tackled this problem by estimating the time-dependent completeness magnitude (Hainzl 2016) and introducing a parametric model: the cumulative distribution function (CDF) of a normal distribution (Ringdal 1975; Ogata & Katsura 1993, 2006; Omi et al. 2013, 2014, 2015a,b; Zhuang et al. 2017; Martinsson & Jonsson 2018) and CDF of an exponential distribution with an upper limit (Mignan 2012; Kijko & Smit 2017; Mignan 2019). The detection function enables the construction of valid estimators in MNAR. Three problems remain to be solved: (i) the resulting estimators are often unstable; (ii) misspecification of the detection function causes bias; (iii) estimation of the detection function is difficult even with a correct model. Problem (i) arises from the simultaneous estimation of the detection function and the distribution of aftershocks. Problem (ii) results from the fact that the bias correction strongly depends on how close the defined detection function is to the true one. Problem (iii) is because some integration is required in the likelihood, which makes estimations difficult in biased sampling problems. In this study, we propose a nonparametric Bayesian estimator to overcome these three problems. Appropriate prior information, considering characteristics of seismic activities in a target area, solves problem (i). A modeling of the detection function based on the technique of the Gaussian Process Regression (GPR), which enables us to estimate an arbitrary continuous function from a given dataset without assuming a specific functional form, solves problems (i) and (ii) simultaneously. The GPR has been accepted widely in recent machine learning research due to its flexibility and wide coverage of function spaces (Rasmussen et al. 2006; de G. Matthews et al. 2018). As for the computation of the model parameters, we propose an efficient Bayesian estimation algorithm utilizing the fact that the distributions of both the Gaussian process (GP) and aftershocks are exponential functions, which are compatible with computation, solving the third problem (iii).

Another advantage of the GPR is that it is capable of evaluating uncertainties or credible intervals of the estimated parameters naturally, which has been difficult in previous studies, in spite of knowing that uncertainty is inevitable in making statistical decisions. In summary, the proposed method can solve the three problems mentioned above and additionally estimate the uncertainties of the parameters.

The remainder of this paper is organized as follows. Section 2 introduces the GPR and proposes a method to estimate parameters for the distribution of aftershocks with a detection function through the GPR. Section 3 validates the proposed method through numerical tests. Section 4 demonstrates the effectiveness of the proposed method by applying it to the catalog data of the 2004 Chuetsu earthquake. Section 5 concludes the present study, including future perspectives.

2 METHODOLOGY

The present paper proposes the use of a detection function based on the GPR to model temporal changes in the detection probability of aftershocks, even immediately after a main shock. This section first gives a brief explanation of the GPR and then introduces the proposed method, especially its theoretical properties and an efficient computational algorithm.

2.1 Gaussian process regression

Recent studies in the solid Earth sciences used the GPR to construct models from given data in the cases that the physical or chemical process that produced the data was unknown or too complex. The GPR estimates a regression function simultaneously with its uncertainty through Bayesian nonparametric estimation. For example, Kuwatani et al. (2018) proposed to apply the GPR to interpolate the observed quantities of chemical compositions along with the radius of a rock. The estimated uncertainty often provides valuable information for observational or experimental designs, such as a suggestion of times and/or places of the next new observations or measurements. The present study adopts the GPR to obtain a nonparametric regression function in the framework of Bayesian estimation.

We first briefly explain the GP, on which the GPR is based. Fundamental statistics mention that, for a random variable, there exists a corresponding distribution that generates random “values”. The GP is an extension of this concept to a random function, i.e., there exists a corresponding distribution that generates random “functions”. The distribution of the GP is usually denoted as $\text{GP}(f_{\text{prior}}(\cdot), \mathcal{K}(\cdot, \cdot))$, where $f_{\text{prior}}(\cdot)$ is the mean function and $\mathcal{K}(\cdot, \cdot)$ is the variance function or “kernel”. The notation $f(\cdot)$ is used in this paper to abbreviate arguments, emphasizing that f is a function. A radial basis function is often chosen among various candidate functions for the variance function or kernel $\mathcal{K}(\cdot, \cdot)$:

$$\mathcal{K}(x_1, x_2) = \phi_1 \exp \left\{ -\frac{(x_1 - x_2)^2}{\phi_2^2} \right\} \quad (\phi_1, \phi_2 > 0), \quad (1)$$

where x_1 and x_2 are arbitrary real numbers. Another reason why this study adopts the radial basis function for the kernel is that it adequately covers an infinite-dimensional function space with only a few hyperparameters. See Rasmussen et al. (2006) for a detailed explanation of the GP, including other kernel functions. Figure 1(a) illustrates three random “functions” generated from a $\text{GP}(f_{\text{prior}}(\cdot), \mathcal{K}(\cdot, \cdot))$ with $f_{\text{prior}}(x) = x^2$, $\phi_1 = 0.3$ and $\phi_2 = 0.3$. For any n points x_1, x_2, \dots, x_n , where n is an arbitrary positive integer, the GP is mathematically equivalent to $\mathbf{f} = (f(x_1), f(x_2), \dots, f(x_n))^{\top}$ computed from a sampled function $f(\cdot)$ that follows a multivariate normal distribution with mean $\mathbf{f}_{\text{prior}} = (f_{\text{prior}}(x_1), f_{\text{prior}}(x_2), \dots, f_{\text{prior}}(x_n))^{\top}$ and variance $\mathcal{K}_n = (\mathcal{K}(x_i, x_j))$. Here (a_{ij}) means a matrix having a_{ij} in its (i, j) -th element, and the superscript \top means transposition. Note that the variance of the value $f(x_i)$ at any point x_i is $\mathcal{K}(x_i, x_i) = \phi_1$, and triple of its standard er-

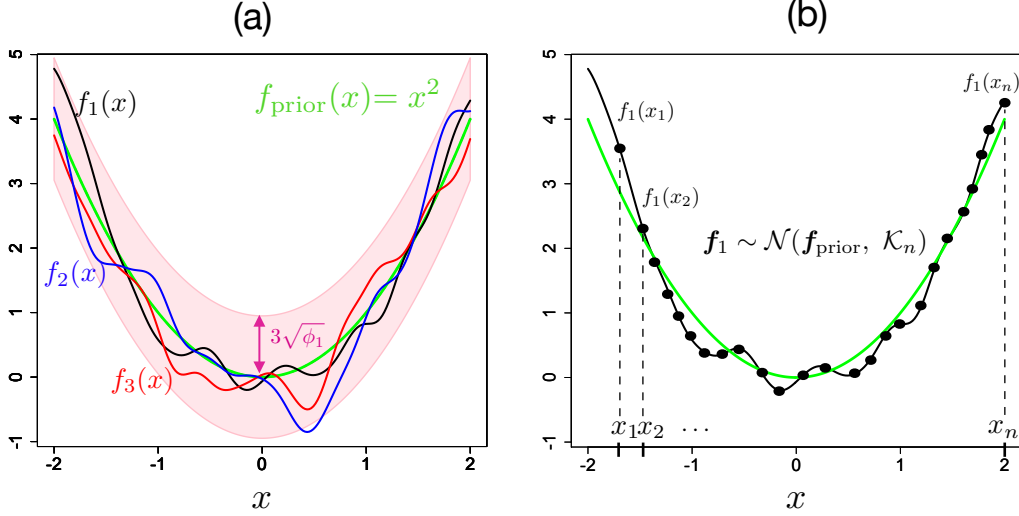


Figure 1. Example of GP: (a) three sampled functions $f_1(x)$ (black line), $f_2(x)$ (blue line), and $f_3(x)$ (red line) generated from a GP with $f_{\text{prior}}(x) = x^2$ (green line), $\phi_1 = 0.3$, and $\phi_2 = 0.1$, and the red shaded zone is three times the standard deviation ($= 3\sqrt{\phi_1}$) from the mean function; (b) values of the function $f_1(x)$ at arbitrary n points x_1, x_2, \dots, x_n . A set of these values forms a function sampled from the distribution of the GP when n goes to infinity.

ror $3\sqrt{\phi_1}$ produces an approximately 99.7% confidence interval for the GP shaded region in red in Figure 1(a). Figure 1(b) indicates that the values of the function $f_1(\cdot)$ (black line in Figure 1(a)) at arbitrary n points x_1, x_2, \dots, x_n follows a multivariate normal distribution $\mathcal{N}(\mathbf{f}_1, \mathcal{K}_n)$, where $\mathbf{f}_1 = (f_1(x_1), f_1(x_2), \dots, f_1(x_n))^\top$. Intuitively speaking, when the number of points n goes to infinity, a set of points forms the function $f_1(\cdot)$ that is a sample from the distribution of the GP. This consideration indicates that the GP is a stochastic process obtained by letting the dimension of a multivariate normal distribution go to infinity.

The GPR is a Bayesian estimation method for a target function using a distribution of the GP as the prior information. Let $\mathbf{x} = (x_1, \dots, x_n)^\top$ and $\mathbf{y} = (y_1, \dots, y_n)^\top$ be sets of explanatory and response variables, respectively, and both are assumed to relate to each other through an unknown regression function $f(\cdot)$, i.e., $y_i = f(x_i)$ ($i = 1, \dots, n$), where n denotes the number of time points. The GPR estimates the function $f(\cdot)$ from a given dataset assuming the kernel function mentioned above. We assume $\text{GP}(f_{\text{prior}}(\cdot), \mathcal{K}(\cdot, \cdot))$ to be a prior distribution of the target function $f(\cdot)$. The mean function $f_{\text{prior}}(\cdot)$ is often assumed to be identically zero since the mean is adjustable by subtracting the sample mean of \mathbf{y} . Estimation of a function $f(\cdot)$ is equivalent to that of the value of $f(x^*)$ at any fixed point x^* , where the superscript “*” is used to discriminate the fixed point from the data points. A posterior distribution of $f^* = f(x^*)$ given a dataset $\mathcal{D} = \{x_1, \dots, x_n, y_1, \dots, y_n\}$ is called the

predictive distribution. The law of total probability yields the predictive distribution as

$$p(f^* | x^*, \mathcal{D}) = \int p(f^* | x^*, \mathbf{f}, \mathcal{D})p(\mathbf{f} | \mathcal{D})d\mathbf{f}, \quad (2)$$

where $p(f^* | x^*, \mathbf{f}, \mathcal{D})$ is the conditional probability density function (PDF) of f^* with the given fixed point x^* , unobserved \mathbf{f} , and the dataset \mathcal{D} , and the PDF $p(\mathbf{f} | \mathcal{D})$ is the prior on \mathbf{f} given by a multivariate normal distribution $\mathcal{N}(\mathbf{f}, \mathcal{K}_n)$ as mentioned above. The predictive distribution becomes a normal distribution again in accordance with the reproductive property. Therefore, the predictive distribution for a point x^* is a normal distribution with mean $\mu_f(x^*)$ and variance $\sigma_f^2(x^*)$ computed as

$$\mu_f(x^*) = \boldsymbol{\kappa}_*^\top \mathcal{K}_n^{-1} \mathbf{y}, \quad \sigma_f^2(x^*) = \kappa_{**} - \boldsymbol{\kappa}_*^\top \mathcal{K}_n^{-1} \boldsymbol{\kappa}_*, \quad (3)$$

where $\mathcal{K}_n = (\mathcal{K}(x_i, x_j))$, $\boldsymbol{\kappa}_* = \{\mathcal{K}(x^*, x_1), \dots, \mathcal{K}(x^*, x_n)\}^\top$ and $\kappa_{**} = \mathcal{K}(x^*, x^*)$. The maximization of the marginal likelihood

$$\prod_{i=1}^n p(y_i | x_i; \phi) = \prod_{i=1}^n \int p(y_i | x_i, \mathbf{f}; \phi)p(\mathbf{f} | x_i; \phi)d\mathbf{f} \quad (4)$$

determines the hyperparameters $\phi = (\phi_1, \phi_2)^\top$, where the integration on the right-hand side is explicitly computable since the integrand given as the product of normal distributions $p(y_i | x_i, \mathbf{f}; \phi)$ and $p(\mathbf{f} | x_i; \phi)$ is again a normal distribution. Figure 2 shows the predictive distributions estimated from six data points with changing hyperparameters ϕ_1 and ϕ_2 in the kernel (eq. 1). As mentioned above, the GPR successfully obtains not only the mean function but also its standard error, i.e., credible interval. Figure 2 also indicates that ϕ_1 and ϕ_2 strongly associate with scale and shape of the regression function, respectively. A comparison between Figures 2(a) and 2(c), or 2(b) and 2(d) indicates that small/large ϕ_1 means a small large/credible interval. Another comparison between Figure 2(a) and 2(b), or 2(c) and 2(d) shows that small/large ϕ_2 means an oscillating/smoothed regression function. These results indicate the importance of deciding the hyperparameters.

2.2 Notation and models

According to the Omori-Utsu law, the aftershock occurrence rate $n(t)$ at elapsed time t from the main shock follows a non-stationary Poisson process (Omori 1894; Utsu 1961):

$$n(t; \boldsymbol{\tau}) = \frac{K}{(t+c)^p}, \quad (5)$$

where $\boldsymbol{\tau}$ is a vector containing all the model parameters, i.e., $\boldsymbol{\tau} = (K, p, c)^\top$. The parameter K controls the level of seismic activity, i.e., large/small K reflects a large/small number of aftershocks. The parameter p is the slope of the occurrence rate on the logarithmic scale. The parameter c characterizes the length of ‘‘capped time’’, which indicates the well-known phenomenon that the occurrence rate is

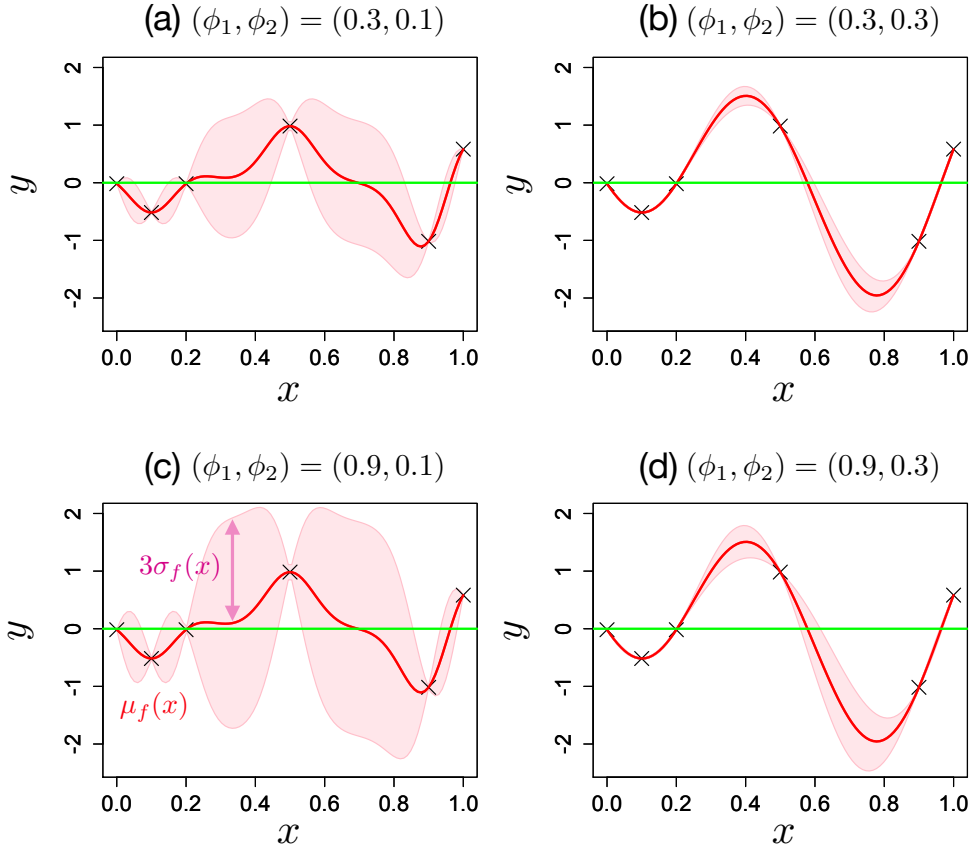


Figure 2. Gaussian process regression applied to six data points (“x”) with different hyperparameters (ϕ_1, ϕ_2) . The green line is the mean function $f_{\text{prior}}(\cdot)$ of the prior distribution, which is assumed to be identically zero, the red curve is the estimated mean $\mu_f(\cdot)$ of the predictive distribution, and the shaded region is the deviation $3\sigma_f(\cdot)$ from the mean of the predictive distribution.

below some level for a while immediately after the main shock (Utsu 1961; Ogata 1983). According to the Gutenberg-Richter law, the intensity rate of the magnitude M is described by an exponential function (Gutenberg & Richter 1944):

$$m(M; b) = A10^{-bM} \propto \exp(-\beta M), \quad (6)$$

where A and b (or $\beta = b \ln 10$) are constants. The parameter b is of most interest since it reflects the intensity rate of the magnitude in the statistical meaning. Combining eqs. (5) and (6), the joint occurrence rate of aftershocks as a function of elapsed time t and magnitude M is represented by the product of $n(t)$ and $m(M)$ as

$$\lambda(t, M; \tau, \beta) = \frac{K'}{(t+c)^p} \beta e^{-\beta(M-M_0)}, \quad (7)$$

where $K' = \beta^{-1}KA \exp(-\beta M_0)$ and M_0 is the magnitude of the main shock used to adjust the scale of K' (Utsu 1970). Note that a unique decomposition into K and A is mathematically impossible,

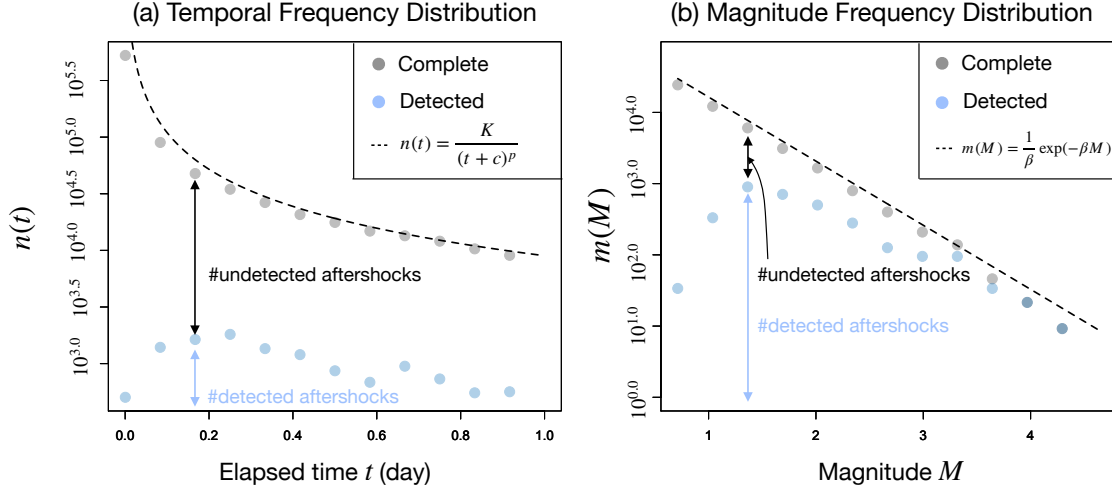


Figure 3. Frequency distribution of (a) elapsed times, and (b) magnitudes on complete and detected aftershocks. Complete data of aftershocks are artificially generated by the Omori-Utsu and the Gutenberg-Richter laws, and detected aftershocks are generated by removing some of the complete data with the probability law.

even if K' is obtained. Resenberg & Jones (1989, 1994) pointed out that an estimation of K' leads to a forecast of seismic activities, so that the unique decomposition problem does not matter in this context. Hereafter, we use K instead of K' for notational simplicity.

An exact count of all aftershocks right after a main shock is very complicated due to contaminations by a number of arriving seismic waves, so that the occurrence rate of aftershocks is almost always underestimated. Figure 3 shows a comparison of artificially generated aftershocks with detected aftershocks, and illustrates how undetected aftershocks distort both the occurrence rate (left) and the distribution of magnitudes (right).

In order to correct the bias, the present study adopts the probit-type detection function, as used in Ringdal (1975), Ogata & Katsura (1993), Ogata & Katsura (2006), Omi et al. (2013, 2014, 2015a,b), and Martinsson & Jonsson (2018):

$$\begin{aligned} \pi(t, M; \mu, s) &= P(\delta = 1 \mid t, M; \mu, s) \\ &= \int_{-\infty}^M \frac{1}{\sqrt{2\pi s^2}} \exp\left\{-\frac{(x - \mu(t))^2}{2s^2}\right\} dx, \end{aligned} \quad (8)$$

where δ is a detection indicator that takes 1/0 if the aftershock is detected/undetected, $\mu(t)$ is the magnitude that makes aftershocks detectable with a probability of 50% at elapsed time t , and s is a scale parameter that determines the steepness of the exponential curve. The detection function $\pi(t, M)$ is the cumulative distribution of a Gaussian normal distribution, and s is the standard deviation of this distribution. Roughly speaking, the function $\mu(t)$ is decreasing with respect to the elapsed time

t because only large aftershocks are detectable immediately after the main shock and even small aftershocks are detectable after enough time has passed.

To distinguish the notations related to complete and detected data, let t_1 and M_1 be the elapsed time and magnitude of a detected aftershock, respectively. The subscript “1” indicates the detected data, i.e., $\delta = 1$. Note that t_1 and M_1 are always available, although the complete data t and M may be unavailable. Supposing that n aftershocks are detected, let the pair of elapsed time from the main shock and the magnitude of the i -th aftershock be (t_{1i}, M_{1i}) ($i = 1, \dots, n$). The thinning operation or the random deletion in point processes (Ogata & Katsura 1993) yields the likelihood function for the detected magnitudes

$$\begin{aligned} & \prod_{i=1}^n L(M_{1i} | t_{1i}; \beta, \mu, s^2) \\ &= \prod_{i=1}^n \frac{e^{-\beta M_{1i}} \pi(t_{1i}, M_{1i}; \mu, s^2)}{\int_{-\infty}^{\infty} e^{-\beta M} \pi(t_{1i}, M; \mu, s^2) dM} \\ &= \prod_{i=1}^n \beta \exp \left\{ -\beta(M_{1i} - \mu(t_{1i})) - \frac{1}{2} \beta^2 s^2 \right\} \pi(t_{1i}, M_{1i}; \mu, s^2), \end{aligned} \quad (9)$$

where the function $\mu(\cdot)$ is assumed to be known, although it is estimated later in practice. Using the estimated $\hat{\beta}$ and \hat{s} obtained by maximizing eq. (9), τ can be estimated by maximizing the log-likelihood function for detected elapsed times within any time interval $(0, T)$ (Ogata & Katsura 1993),

$$\ln L = \sum_{0 < t_{1i} < T} \ln \nu(t_{1i}; \tau, \mu(t_{1i}), \hat{\beta}, \hat{s}) - \int_0^T \nu(t; \tau, \mu(t), \hat{\beta}, \hat{s}) dt, \quad (10)$$

where $\nu(t)$ is an intensity function for detected data defined by

$$\begin{aligned} & \nu(t; \tau, \mu(t), \beta, s) \\ &= \int_{-\infty}^{\infty} \lambda(t, M; \tau, \beta) \pi(t, M; \mu, s) dM \\ &= \frac{K}{(t+c)^p} \exp \left\{ -\beta(\mu(t) - M_0) + \frac{1}{2} \beta^2 s^2 \right\}. \end{aligned} \quad (11)$$

However, the serious problem that $\mu(\cdot)$ is unknown remains. In frequentist ways, Martinsson & Jonsson (2018) and Mignan (2019) proposed a mixture detection function of parametric models. Although the mixture detection function is flexible and approximates the true detection function well, either misspecification of the parametric models or the number of mixture components causes biased estimates. As for nonparametric models, Ogata & Katsura (1993) applied a B-spline basis function to $\mu(\cdot)$, and Ogata & Katsura (2006) proposed a specific parametric model based on the 2003 Miyagi-Ken-Oki earthquake as

$$\mu(t) = a_0 + a_1 \exp \{ -\alpha([\cdot] + \ln t)^\gamma \}, \quad (12)$$

where a_0 , a_1 , α , and γ are parameters to be estimated and $[\cdot]$ is the ceiling function. Recently,

Omi et al. (2013) proposed a flexible nonparametric Bayesian estimation. They assumed a prior on $\mu(t_{1i})$ ($i = 1, \dots, n$) as

$$(\mu_1, \dots, \mu_n) \sim p(\mu_1, \mu_2) \prod_{i=1}^{n-2} \frac{1}{\sqrt{2\pi V}} \exp\left(-\frac{(\mu_{i+2} - 2\mu_{i+1} - \mu_i)^2}{2V}\right), \quad (13)$$

where V is a hyperparameter and $p(\mu_1, \mu_2)$ is a constant, and μ_i ($i = 1, \dots, n$) is estimated by the posterior mean. This prior indicates that the mean of each μ_n is a point apart from μ_{n-1} with a distance of $(\mu_{n-1} - \mu_{n-2})$ given the values μ_{n-1} and μ_{n-2} . Their method does not require any specification of $\mu(\cdot)$ and it can naturally incorporate the prior information of β , which makes estimates considerably stable. The posterior distribution of β can be estimated in the same aftershock area that occurred before the main shock. Also, it is difficult to evaluate the credibility of $\mu(\cdot)$.

2.3 Estimation of β , s^2 , and $\pi(\cdot)$

Figure 4(a) shows a graphical model for complete data, which illustrates how the data, parameters, and hyperparameters relate to each other in accordance with the Omori-Utsu law, the Gutenberg-Richter law, and the detection function. Since the complete data are not available, we construct a likelihood based on the detected data M_1 given t_1 , as shown in Figure 4(b). The distribution of M_1 given t_1 is already derived in eq. (9). Once the graphical model for the detected data is obtained, it can be realized that the relation among M_1 , μ , and t_1 is exactly the same as in the regression: each input x , the regression $f(\cdot)$, and output y corresponds to t_1 , $\mu(\cdot)$, and M_1 , respectively. Based on this idea, we put the GP prior on $\mu(\cdot)$ and consider a nonparametric Bayesian estimation. However, unlike the GPR explained in Section 2.1, the distribution derived in eq. (9) is not a normal distribution, and the predictive distribution shall be more complicated.

In this study, we put a GP prior on the ‘‘function’’ $\mu(\cdot)$, not on the ‘‘points’’ $\mu(t_{1i})$ ($i = 1, \dots, n$). The GP prior leads to an explicit form of the posterior distribution of the hyperparameters and the predictive distribution of $\mu(\cdot)$, as seen in the following discussion. The prior for $\mu(\cdot)$ can be denoted as

$$\mu \sim \text{GP}(\mu_{\text{prior}}(\cdot), \mathcal{K}(\cdot, \cdot)), \quad (14)$$

where \mathcal{K} is defined as

$$\mathcal{K}(x_1, x_2) = \phi_0 + \phi_1 \exp\left\{-\frac{(x_1 - x_2)^2}{\phi_2^2}\right\} \quad (\phi_1, \phi_2 > 0). \quad (15)$$

The first term ϕ_0 in eq. (15) is added to the usual kernel eq. (1) to make the matrix \mathcal{K}^{-1} always nonsingular. A subjectively small value, e.g., 10^{-7} , is set to ϕ_0 for a stable estimation of the other parameters. The prior $\mu_{\text{prior}}(\cdot)$ should be a function except for identically zero in this case since adjusting the mean of the prior as in the standard GPR is impossible. We propose to use the Ogata

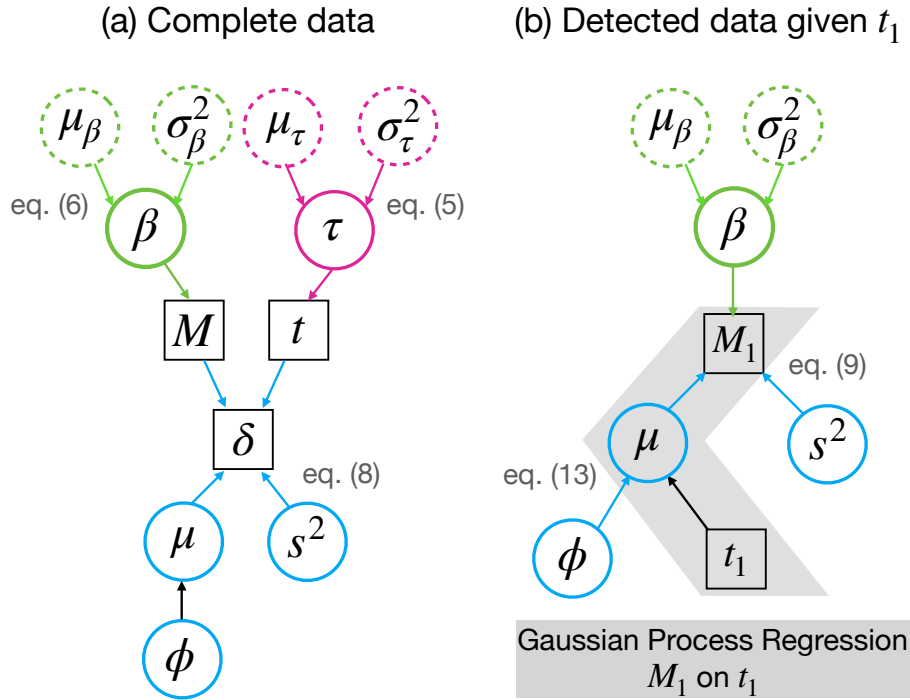


Figure 4. Graphical models on (a) complete data; (b): detected data given t_1 . Each square, circle, and dotted circle indicates data, parameters, and subjective hyperparameters, respectively. Each green, red, and blue color indicates the relation by the Gutenberg-Richter law, the Omori-Utsu law, and the detection function, respectively.

model (eq. 12) because of the prior information of $\mu(\cdot)$ since the model successfully represents the detection function on average, although representing small oscillations is difficult due to the limited number of parameters (Omi et al. 2013).

In summary, the parameters to be estimated are $\theta = (\beta, s^2, \phi_1, \phi_2)^\top$. We apply exactly the same subjective priors as Omi et al. (2015b) that are estimated in Omi et al. (2015a) by fitting the Omori-Utsu and the Gutenberg-Richter laws to 38 aftershock sequences in Japan from the JMA catalog. Let $\beta \sim p(\beta) = \mathcal{N}(1.96, 0.34^2)$ be the estimated prior distribution for β . The posterior distribution of $\theta = (\beta, s^2, \phi_1, \phi_2)^\top$ and the predictive distribution of $\mu(\cdot)$ are computable as follows (see Appendix for the proofs).

- Posterior distribution of $\boldsymbol{\theta} = (\beta, s^2, \phi_1, \phi_2)^\top$:

$$\begin{aligned}
& p(\boldsymbol{\theta} \mid \mathcal{D}) \\
& \propto p(\beta) \int p(\mathbf{M}_1 \mid \mathbf{t}_1; \beta, \boldsymbol{\mu}, s^2) p(\boldsymbol{\mu} \mid \mathbf{t}_1; \phi_1, \phi_2) d\boldsymbol{\mu} \\
& = \beta^n \exp \left\{ -\beta(\mathbf{M}_1 - \boldsymbol{\mu}_{\text{prior}})^\top \mathbf{1}_n - \frac{1}{2} \beta^2 \mathbf{1}_n^\top (s^2 I_n - \mathcal{K}_n) \mathbf{1}_n \right\} \\
& \quad \times p(\beta) \int_{\mathcal{M}} \mathcal{N}(\mathbf{x}; \tilde{\boldsymbol{\mu}}_n, \tilde{\mathcal{K}}_n) d\mathbf{x},
\end{aligned} \tag{16}$$

where $\mathcal{M} = \otimes_{i=1}^n \{x_i \leq M_{1i}\}$ is the integration interval, $\otimes_{i=1}^n$ is the direct product of the n sets $\{x_i \leq M_{1i}\}$ ($i = 1, \dots, n$), $\tilde{\boldsymbol{\mu}}_n = \boldsymbol{\mu}_{\text{prior}} + \beta \mathcal{K}_n \mathbf{1}_n$, $\mathbf{1}_n$ is the n -dimensional vector that has one in all of its elements, $\tilde{\mathcal{K}}_n = \mathcal{K}_n + s^2 I_n$, I_n is the n -dimensional identity matrix, and $\mathcal{N}(\mathbf{x}; \boldsymbol{\mu}, \Sigma)$ is the PDF of the normal distribution, with mean $\boldsymbol{\mu}$ and variance Σ . One reasonable estimator of $\boldsymbol{\theta}$ is the unique maximizer of eq. (16), called a maximum a posteriori (MAP) estimator.

- Predictive distribution of $\mu(\cdot)$:

$$\begin{aligned}
& p(\mu^* \mid t_1^*, \mathcal{D}) \\
& = \int p(\mu^* \mid t_1^*, \boldsymbol{\mu}, \mathcal{D}) p(\boldsymbol{\mu} \mid \mathcal{D}) d\boldsymbol{\mu}
\end{aligned} \tag{17}$$

$$= \mathbb{E}_{\text{trunc}} \left\{ \mathcal{N}(\mu^*; D^*(\mathbf{X}), (\tau^*)^2) \right\}, \tag{18}$$

where

$$D^*(\mathbf{x}) = (\mathbf{x} + s^2 \mathcal{K}_n^{-1} \tilde{\boldsymbol{\mu}}_n)^\top \left\{ (\tau^*)^2 \tilde{\mathcal{K}}_n^{-1} + \tilde{\mathcal{K}}_n^{-1} \boldsymbol{\kappa}_* \boldsymbol{\kappa}_*^\top \tilde{\mathcal{K}}_n^{-1} \right\} \frac{\boldsymbol{\kappa}_*}{\kappa_{**}}, \tag{19}$$

$\boldsymbol{\kappa}_* = (\mathcal{K}(t_1^*, t_{11}), \dots, \mathcal{K}(t_1^*, t_{1n}))^\top$, $\kappa_{**} = \mathcal{K}(t_1^*, t_1^*)$, and $(\tau^*)^2 = \kappa_{**} - \boldsymbol{\kappa}_*^\top \tilde{\mathcal{K}}_n^{-1} \boldsymbol{\kappa}_*$. The expectation $\mathbb{E}_{\text{trunc}}$ is on a variable $\mathbf{X} \sim \mathcal{TN}(\tilde{\boldsymbol{\mu}}_n, \tilde{\mathcal{K}}_n, \mathcal{M})$, where $\mathcal{TN}(\boldsymbol{\mu}, \Sigma, \mathcal{R})$ is the truncated multivariate normal distribution with mean $\tilde{\boldsymbol{\mu}}_n$, variance $\tilde{\mathcal{K}}_n$, bounded by the region \mathcal{R} . In particular, the mean and the variance of the predictive distribution are $D^*(\boldsymbol{\xi})$ and $(\tau^*)^2$, where

$$\boldsymbol{\xi} = \mathbb{E}_{\text{trunc}}(\mathbf{X}). \tag{20}$$

The symbol “*” explicitly represents that the variable depends on t_1^* .

- Predictive distribution of detection probability $\pi(\cdot)$:

$$\begin{aligned}
& \pi^*(M_1^*, t_1^*) \\
& = \int P(\delta = 1 \mid M_1^*, \mu^*, \mathcal{D}) p(\mu^* \mid t_1^*, \mathcal{D}) d\mu^* \\
& = \mathbb{E}_{\text{trunc}} \left\{ \Psi \left(\frac{M_1^* - D^*(\mathbf{X})}{\sqrt{s^2 + (\tau^*)^2}} \right) \right\},
\end{aligned} \tag{21}$$

where $\Psi(\cdot)$ is the cumulative distribution function of the standard normal distribution, i.e., $\mathcal{N}(0, 1)$.

The integrations in eqs. (18), (20), and (21) are computable by the Monte Carlo method since they involve expectations on the known truncated multivariate normal distribution $\mathcal{TN}(\tilde{\boldsymbol{\mu}}_n, \tilde{\mathcal{K}}_n, \mathcal{M})$.

However, computation of the integration in the posterior distribution (eq. 16) is more difficult. We provide an efficient computational algorithm to obtain the posterior samples of the hyperparameter θ , instead of maximizing the posterior distribution (eq. 16) directly.

2.4 Estimation of τ

Recall that the log-likelihood function for τ is given in eq. (23), but $\mu(\cdot)$ is unknown in the intensity function (eq. 11). Ogata & Katsura (1993) and Omi et al. (2013) replaced $\mu(\cdot)$ with the MAP estimator. We propose to use an estimated mean of the predictive distribution for $\mu(\cdot)$ (eq. 20). For example, $(\mu(t_{1i}), \dots, \mu(t_{1n}))$ is estimated by $(\hat{\xi}_1, \dots, \hat{\xi}_n)$, where $\hat{\xi} = \hat{\mathbb{E}}_{\text{trunc}}(\mathbf{X})$ is an estimated mean of the predictive distribution with its sample mean generated from $\mathcal{TN}(\tilde{\mu}_n, \tilde{\mathcal{K}}_n, \mathcal{M})$. We also apply the following priors for τ estimated in Omi et al. (2015a) as explained in Section 2.3:

$$\ln K \sim \mathcal{N}(-4.86, 1.60^2), \quad p \sim \mathcal{N}(1.05, 0.13^2), \quad \ln c \sim \mathcal{N}(-4.02, 1.42^2). \quad (22)$$

Let $p(\tau)$ be product of the three distributions in eq. (22). Then, our estimating equation for τ is

$$\log p(\tau) + \sum_{0 < t_{1i} < T} \ln \nu(t_{1i}; \tau, \hat{\xi}_i, \hat{\beta}, \hat{s}) - \int_0^T \nu(t; \tau, \mu(t), \hat{\beta}, \hat{s}) dt. \quad (23)$$

As for the integration of the third term in eq. (23), we use a left Riemann sum, discretizing the interval $[0, T]$ into 10^4 meshes having the same interval. The predictive distribution of $\mu(\cdot)$ enables us to estimate corresponding $(\mu_1, \dots, \mu_{10^4})$, including data points except for detected aftershocks in a similar way to estimate ξ , unlike the model by Omi et al. (2014), in which only $(\mu(t_{1i}), \dots, \mu(t_{1n}))$ is estimable. Our method can precisely evaluate the integration in the third term in eq. (23).

2.5 Computational algorithm

Both the posterior distribution and the predictive distribution involve integration on the multivariate normal distribution over an n -dimensional hyperrectangle \mathcal{M} . Since an explicit computation of the integral is difficult, even when the dimension is low (Genz & Bretz 2009), we divide the estimation into two steps: (i) estimation of hyperparameters θ ; (ii) computation of mean and variance of the predictive distribution.

In step (i), the data-augmentation method (Tanner & Wong 1987) is applied to obtain samples from the posterior distribution of θ . Regarding variable \mathbf{x} in eq. (16) as a latent variable yields another representation of the posterior distribution as

$$p(\theta | \mathcal{D}) = \int_{\mathcal{M}} p(\theta, \mathbf{x} | \mathcal{D}) d\mathbf{x}, \quad (24)$$

where

$$\begin{aligned} p(\boldsymbol{\theta}, \mathbf{x} \mid \mathcal{D}) \\ = \beta^n \exp \left\{ -\beta(\mathbf{M}_1 - \boldsymbol{\mu}_{\text{prior}})^\top \mathbf{1}_n - \frac{1}{2} \beta^2 \mathbf{1}_n^\top (s^2 I_n - \mathcal{K}_n) \mathbf{1}_n \right\} \mathcal{N}(\mathbf{x}; \tilde{\boldsymbol{\mu}}_n, \tilde{\mathcal{K}}_n). \end{aligned} \quad (25)$$

In accordance with the Gibbs sampling, augmented data can be sampled via the following two steps:

- (i) Draw $\mathbf{x} \sim p(\mathbf{x} \mid \boldsymbol{\theta}, \mathcal{D}) = \mathcal{TN}(\mathbf{x}; \tilde{\boldsymbol{\mu}}_n, \tilde{\mathcal{K}}_n, \mathcal{M})$;
- (ii) Draw $\boldsymbol{\theta} \sim p(\boldsymbol{\theta} \mid \mathbf{x}, \mathcal{D}) \propto p(\mathcal{D}, \mathbf{x} \mid \boldsymbol{\theta})p(\boldsymbol{\theta} \mid \boldsymbol{\theta}_0)$,

We apply the Gibbs sampling to obtain samples from the truncated normal distribution (Geweke 1991, 2005) and use the package `trmvtnorm` of the R programming language (Wilhelm & Manjunath 2015) in the practical programming. As for sampling of $\boldsymbol{\theta}$, the classical random walk MCMC (Markov Chain Monte Carlo) method (Metropolis et al. 1953) works with a normal distribution as the proposal distribution. By repeating the two steps alternately, the obtained $\boldsymbol{\theta}$ becomes samples from the posterior of $\boldsymbol{\theta}$. Hyperparameters are estimated as the median of obtained samples. Once samples of \mathbf{x} are obtained, $\boldsymbol{\xi} = \mathbb{E}_{\text{trunc}}(\mathbf{X})$ can be estimated by its sample mean. The mean of the predictive distribution of $\mu(\cdot)$ is computable with the estimated $\boldsymbol{\xi}$ by $D^*(\boldsymbol{\xi})$ given in eq. (19) and the variance is computable by $(\tau^*)^2$.

3 NUMERICAL EXPERIMENTS

We conducted numerical tests for the two cases of synthetic observation data to validate the performance of the proposed method. The assumed true values for the parameters in the Omori-Utsu and the Gutenberg-Richter laws that are used to generate the two synthetic datasets are

$$b = 0.9, \quad \ln K = -3.329, \quad p = 1.100, \quad \ln c = -5.809. \quad (26)$$

The magnitude of the main shock is assumed to be $M_0 = 6.0$.

The true detection functions modeled by eq. (8) in the two cases are

$$\begin{aligned} \text{Case 1. } \mu(t) &= \frac{5}{1 + \exp(15t)} + 1.4; \\ \text{Case 2. } \mu(t) &= \frac{5}{1 + \exp(15t)} + 1.4 - \sum_{j=1}^4 \nu_j(t), \end{aligned}$$

where the same scale parameter defined in eq. (8) is assumed as $s = 0.2$ for both cases,

$$\nu_j(t) = \frac{\sin \{15(\log_{10} t + 1.8 - 0.4j)\}}{j + 2} I \{15|\log_{10} t + 1.8 - 0.4j| \leq \pi\}, \quad (27)$$

and $I\{A\}$ is the indicator function that is one if an event A is true, otherwise it is zero. Figure 4 shows the true detection functions for both cases. Case 1 supposes an ordinary situation that the detectable magnitude of aftershocks monotonically decreases as the signal-to-noise ratio recovers with elapsed time t from the main shock. Case 2 supposes a more complicated situation that several large

aftershocks excite many subsequent aftershocks, which temporarily decrease the signal-to-noise ratio (Omi et al. 2013). We first estimated the predictive distribution of $\mu(\cdot)$ and β , and their credibility with the data of aftershocks detected within $t \leq 3\text{h}$, 6h , 12h , and 24h . With the estimated $\hat{\mu}(\cdot)$, $\hat{\beta}$, and $\hat{\sigma}$, τ is estimated by the method stated in Section 2.4.

Figure 5 shows the estimated predictive distribution of $\hat{\mu}(\cdot)$. The mean of the predictive distribution is overall close to the true $\mu(\cdot)$ and inside a region within $3\hat{\sigma}(\cdot)$, where $\hat{\sigma}(\cdot)$ is the estimated standard error of $\hat{\mu}(\cdot)$. In Case 2, it was difficult to detect the first peak in $\mu(\cdot)$ due to the insufficient number of detected aftershocks, but the other peaks could be successfully detected. It is worth noting that even if the mean of the prior distribution (green line) is not very similar to the true one (black dashed line), especially in Case 2, the predictive distribution reproduces the true $\mu(\cdot)$ considerably well. The method of Omi et al. (2013) also works well after some time elapses, but it overfits with time when more aftershocks are detected, so that it is biased in time when less aftershocks are detected, such as $t \leq 3\text{h}$. Table 1 shows the L_2 distance of between the estimated $\mu(\cdot)$ and the true one:

$$L_2(t) = \int_0^t (\hat{\mu}(s) - \mu(s))^2 ds \quad (28)$$

at $t = 3/24, 6/24, 12/24$, and $24/24$ (day), which is approximately computed by a left Riemann sum, discretizing the interval $[0, t]$ into 10^4 meshes having the same interval. Estimated $\hat{\mu}(\cdot)$ with the Ogata model is the closest to the true one in Case 1, which is an obvious result showing that the Ogata model is appropriate for such a smoothed $\mu(\cdot)$. It is to be noted in Case 1 that the proposed model obtained a more smoothed $\mu(\cdot)$ having a smaller L_2 distance compared to that estimated by the Omi method, indicating that the proposed model appropriately avoided overfitting. In Case 2, the Omi and the proposed models, both of which can extract rapid temporal variations in $\mu(\cdot)$, naturally obtained smaller L_2 distances than the Ogata model. The remarkable point in Case 2 is that the proposed model obtained the smallest L_2 distance among the three models, indicating that the proposed model firmly extracted the temporal variation in the true $\mu(\cdot)$. In summary, the proposed model is as robust as the Ogata model in Case 1 and more flexible than the Omi method for estimating the complicated $\mu(\cdot)$ in Case 2.

Table 2 summarizes the estimated \hat{b} and $\hat{\tau}$. The resulting b within $t \leq 3\text{h}$ and 6h in Case 1 overestimates the true value $b = 0.9$. This overestimation is not due to the imperfectness of the proposed method but due to the sampling bias. In fact, as the elapsed time increases, the mean of posterior samples converges to the true value, and the width of the credible interval becomes shorter.

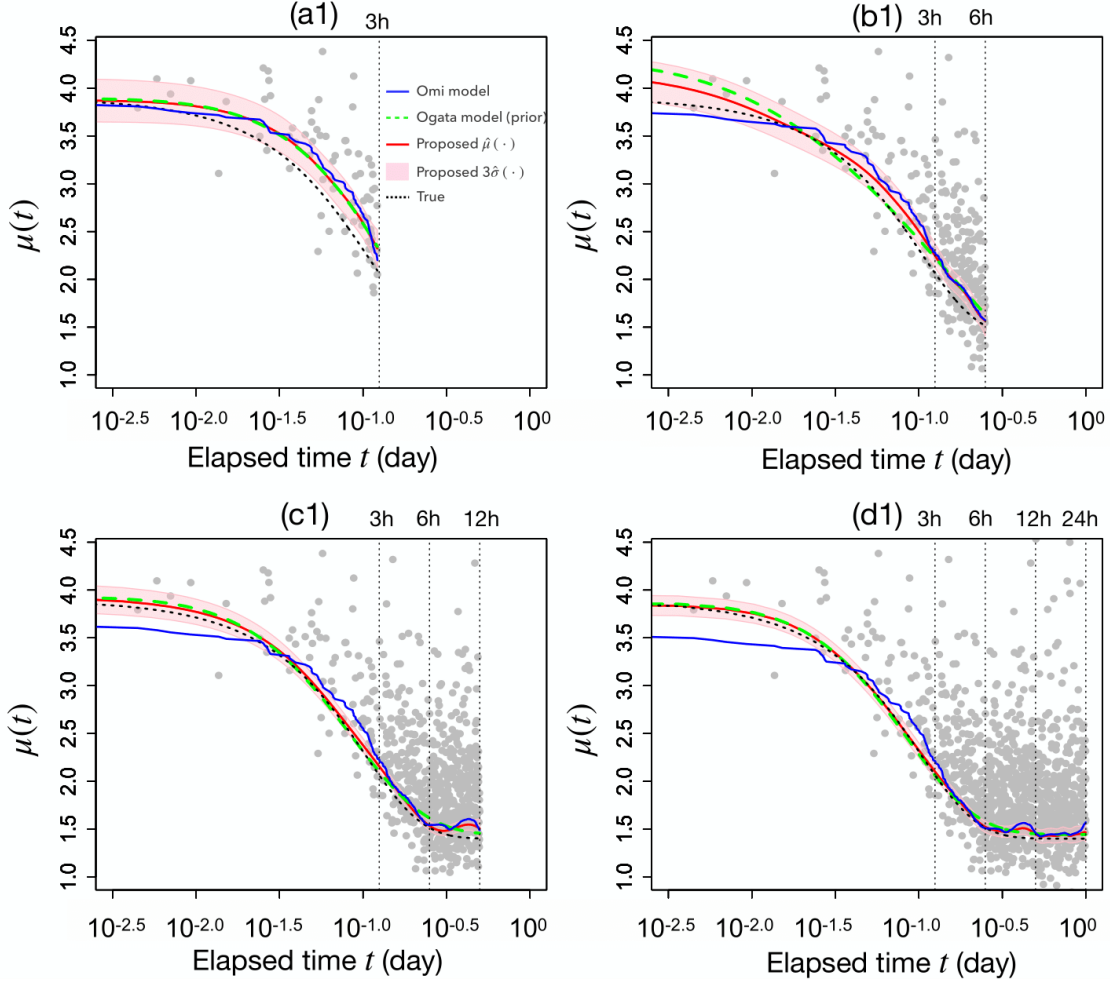


Figure 5. Results of numerical tests to validate the proposed method in Case 1. The blue line indicates the estimated $\mu(\cdot)$ by the method of Omi et al. (2014), the green line indicates the prior of the mean of the predictive distribution $\mu_{\text{prior}}(\cdot)$ estimated by the method of Ogata & Katsura (2006), and the red line indicates the estimated mean $\hat{\mu}(\cdot)$ with the estimation error $\hat{\mu}(\cdot) \pm 3\hat{\sigma}(\cdot)$, shown by the red shaded zone, as compared to the true mean $\mu(\cdot)$, shown by the dashed line, assuming that data are available for (a1) $t \leq 3\text{h}$, (b1) $t \leq 6\text{h}$, (c1) $t \leq 12\text{h}$, and (d1) $t \leq 24\text{h}$ from the main shock.

4 REAL DATA ANALYSIS

The proposed method was applied to the real catalog data related to the 2004 Chuetsu earthquake, officially released from the Japan Meteorological Agency (JMA). The 2004 Chuetsu earthquake (magnitude $M_0 = 6.8$, epicenter $37^\circ 17' 30''$ N, $138^\circ 52' 00''$ E) occurred in Niigata prefecture, Japan at 17h56m on October 23, 2004 (JST). Figure 6 shows the spatial distribution of aftershocks that occurred within $t \leq 24\text{h}$ from the main shock. The dataset is perfectly the same as used in Omi et al. (2015b), in which the aftershocks occurred in a rectangular area. Lengths four times as long as those of the Utsu-Seki aftershock zone for latitudinal and longitudinal directions were selected. The Utsu-

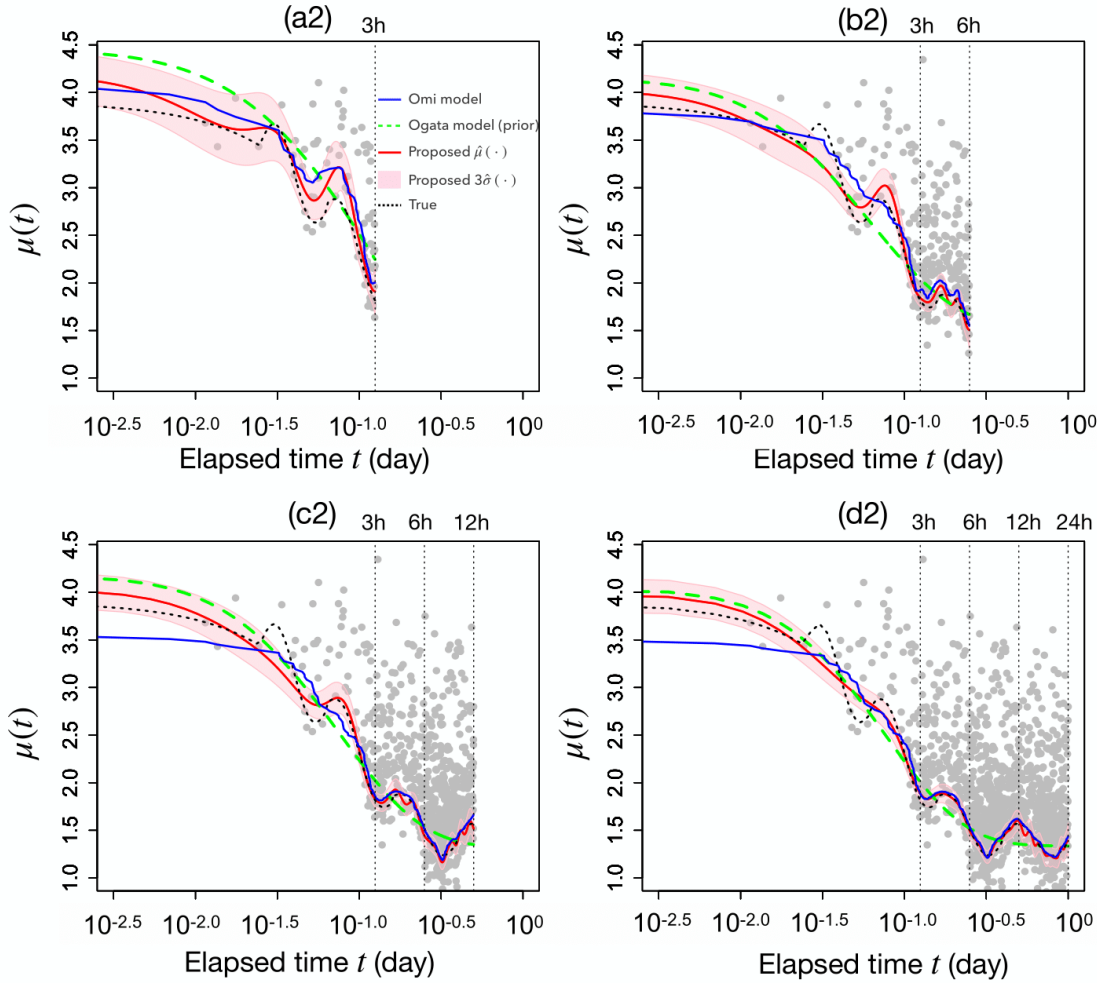


Figure 5 (continued). Results of numerical tests to validate the proposed method in Case 2. See the caption of the previous figure for detailed explanations.

Seki aftershock zone is a rectangular region, in which the epicenter is located at the center, having the angle lengths of $2D(M_0)$ for both latitudinal and longitudinal directions, where $D(M_0)$ is the Utsu-Seki aftershock zone length, defined using the magnitude of the main shock M_0 as $D(M_0) = 0.01 \times 10^{0.5M_0 - 1.8}$ (Utsu 1969). In the case of the 2004 Chuetsu earthquake, $D(M_0)$ is $23'53''$.

Figure 7 shows the results of the application to the real catalog data. Following the same procedure as in the numerical tests in Section 3, the proposed method estimates the mean $\hat{\mu}(\cdot)$ of the predictive distribution with the standard error $\hat{\sigma}(\cdot)$ starting from the prior $\mu_{\text{prior}}(\cdot)$, assuming data availability for $t \leq 3\text{h}$, 6h , 12h , and 24h from the main shock. The magnitudes of aftershocks range from 0.8 to 6.6 with elapsed time within $t \leq 24\text{h}$.

An enormous number of large aftershocks would cause and self-excite a sudden decrease of the detection rate. The proposed method can extract such a hidden structure owing to the wide repre-

Table 1. L_2 distance (eq. 28) of estimated $\mu(\cdot)$ for Ogata, Omi, and proposed methods in Cases 1 and 2. Bold value indicates the closest method to the true $\mu(\cdot)$.

| Elapsed time | Case 1 | | | | Case 2 | | | |
|--------------|--------------------|--------------------|---------------------|---------------------|--------------------|--------------------|---------------------|---------------------|
| | $t \leq 3\text{h}$ | $t \leq 6\text{h}$ | $t \leq 12\text{h}$ | $t \leq 24\text{h}$ | $t \leq 3\text{h}$ | $t \leq 6\text{h}$ | $t \leq 12\text{h}$ | $t \leq 24\text{h}$ |
| Ogata | 0.046 | 0.016 | 0.007 | 0.001 | 0.042 | 0.040 | 0.029 | 0.019 |
| Omi | 0.085 | 0.036 | 0.019 | 0.009 | 0.082 | 0.019 | 0.011 | 0.007 |
| Proposed | 0.053 | 0.021 | 0.007 | 0.002 | 0.039 | 0.013 | 0.007 | 0.004 |

sentability of functions of the GPR. The estimated $\mu(\cdot)$ by the method of Omi et al. (2013) shown in Figure 7 for comparison seems to be unstable, depending on the number of detected aftershocks. When available data are insufficient (Figures 7(a) and 7(b)), the method of Omi et al. (2013) also captures some oscillations, but after time elapses (Figures 7(c) and 7(d)), the resulting detection function becomes too smooth. A similar phenomenon is also seen in Figure 3 in Omi et al. (2013). On the other hand, the proposed method always obtains a stable estimation, independent of the number of aftershocks owing to the wide representability of functions of the GPR, as stated above. To investigate the large difference in the estimates of $\mu(t)$ at $t \leq 1\text{h}$, we utilized the catalog of aftershocks proposed by Enescu et al. (2007). This catalog contains the aftershocks visually detected within $t \leq 0.73\text{h}$ from six High Sensitivity Seismograph Network (Hi-net) stations, shown in Figure 6, which are not included in the JMA catalog. Figure 8, in which the visually detected aftershocks are added to Figure 7(d), supports the validity of the negative peak at $t = 0.47\text{h}$ and the positive peak at $t = 0.65\text{h}$ in $\mu(t)$

Table 2. Estimated posterior means and standard errors of b and $\tau = (K, c, p)^\top$ in Cases 1 and 2

| Elapsed time | Case 1 | | | | Case 2 | | | |
|--------------|---------------------------|---------------------------|---------------------------|---------------------------|---------------------------|---------------------------|---------------------------|---------------------------|
| | $t \leq 3\text{h}$ | $t \leq 6\text{h}$ | $t \leq 12\text{h}$ | $t \leq 24\text{h}$ | $t \leq 3\text{h}$ | $t \leq 6\text{h}$ | $t \leq 12\text{h}$ | $t \leq 24\text{h}$ |
| # of data | 78 | 289 | 680 | 1091 | 93 | 278 | 733 | 1168 |
| b | 1.060 (± 0.073) | 1.035 (± 0.056) | 0.974 (± 0.048) | 0.936 (± 0.031) | 0.966 (± 0.078) | 0.895 (± 0.062) | 0.861 (± 0.040) | 0.877 (± 0.033) |
| $\ln K$ | -6.350 (± 0.292) | -6.089 (± 0.163) | -4.636 (± 0.092) | -3.556 (± 0.051) | -5.771 (± 0.257) | -4.644 (± 0.166) | -3.472 (± 0.085) | -3.024 (± 0.048) |
| p | 1.115 (± 0.111) | 1.231 (± 0.086) | 1.077 (± 0.063) | 1.031 (± 0.044) | 1.084 (± 0.090) | 1.068 (± 0.082) | 0.986 (± 0.055) | 1.047 (± 0.041) |
| $\ln c$ | -5.355 (± 0.672) | -5.873 (± 0.719) | -5.950 (± 0.727) | -5.827 (± 0.705) | -6.823 (± 0.863) | -6.348 (± 0.907) | -6.603 (± 0.896) | -6.229 (± 0.831) |

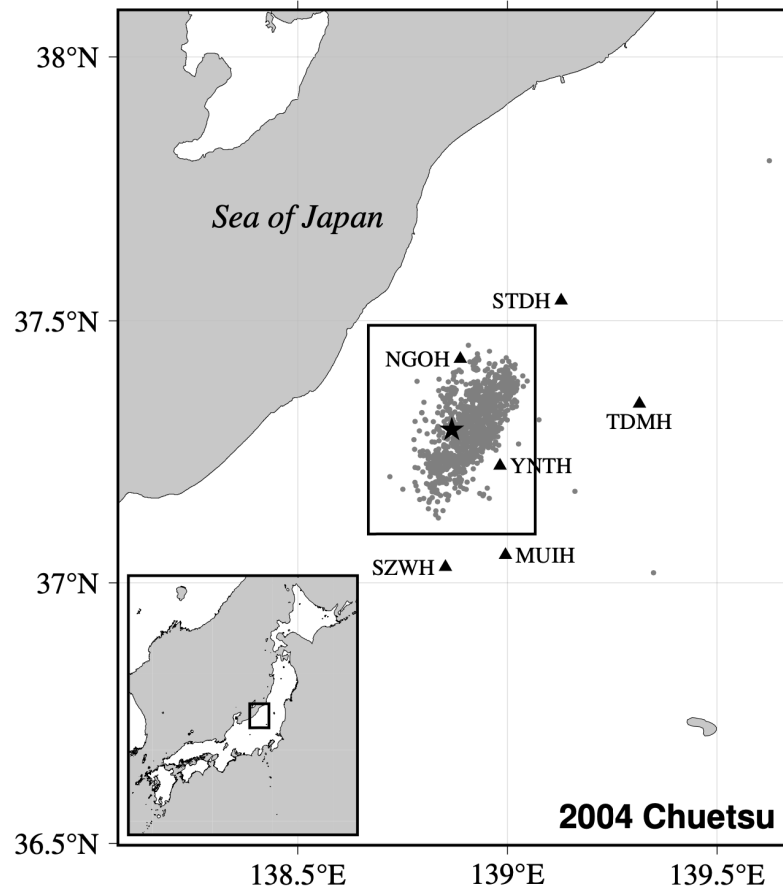


Figure 6. Spatial distribution of aftershocks (circle) within $t \leq 24$ h from the main shock (star) of the 2004 Chuetsu earthquake, officially released by JMA. The small rectangle is the Utsu-Seki aftershock zone, the center of which is the epicenter of the main shock, having the angle lengths of $2D(M_0)$ for both latitudinal and longitudinal directions, where $D(M_0)$ is the Utsu-Seki aftershock zone length. The catalog of aftershocks detected at six Hi-net observatories (triangles) proposed by Enescu et al. (2007) was used to validate the proposed method.

estimated by the proposed method. The negative peak reflects the fact that small aftershocks down to $M = 2.0$ are detected probably due to a temporal decrease in seismic activities, and the positive peak reflects the increase in the lower bound of observed magnitudes.

Figure 9(a) shows the estimated predictive detection function (eq. 21) in the case of the 2004 Chuetsu earthquake, and Figure 9(b) plots its cross-sections at the magnitudes $M = 0.8, 1.8, 2.3,$ and 2.8 . These magnitudes correspond to the minimum (0th percentile), 25th percentile, median (50th percentile), and 75th percentile in the catalog data, where the q th-percentile is the magnitude below which $q\%$ of all the aftershocks are found. Figure 9(a) shows that the detection function intensively fluctuates, unlike in the numerical experiments, which is thought to reflect the rapid temporal variation of

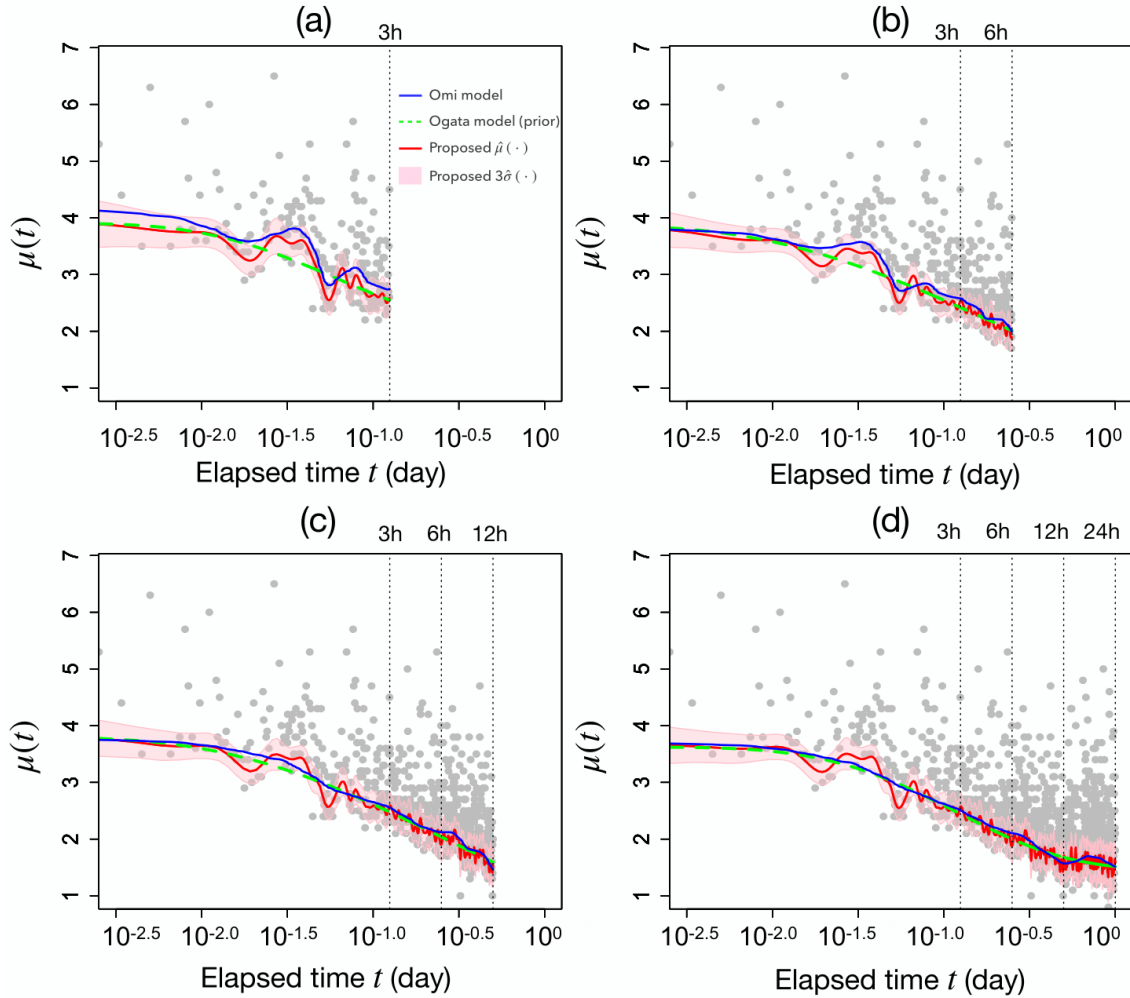


Figure 7. Results of application of our method to the 2004 Chuetsu earthquake based on the JMA catalog. The blue line indicates the estimated $\mu(\cdot)$ by the method of Omi et al. (2014), the green line indicates the prior of the mean of the predictive distribution $\mu_{\text{prior}}(\cdot)$ estimated by the method of Ogata & Katsura (2006), and the red line indicates the estimated mean $\hat{\mu}(\cdot)$ with the estimation error $\hat{\mu}(\cdot) \pm 3\hat{\sigma}(\cdot)$, shown by the red shaded zone, assuming that data are available for (a) $t \leq 3\text{h}$, (b) $t \leq 6\text{h}$ (c) $t \leq 12\text{h}$, and (d) $t \leq 24\text{h}$ from the main shock.

the seismic activities. Figure 9(b) indicates that the minimum magnitude of the complete recording M_c is 2.3 (75th percentile) after $t \geq 0.4$ (day). Wiemer & Wyss (2000) proposed a method to estimate M_c by the smallest magnitude at which 90% of the aftershocks can be modeled by the Gutenberg-Richter law. Enescu et al. (2007) obtained $M_c = 1.8$ at $t = 0.5$ (day) by applying the procedure of Wiemer & Wyss (2000) to the 2004 Chuetsu Earthquake, which seems to be consistent with Figure 9(b). Table 3 summarizes the mean and the standard error of the posterior distribution of b within an elapsed time of $t \leq 3\text{h}$, 6h , 12h , and 24h . The estimates for the b are stable, irrespective of the time available, but the estimated p at $t \leq 12\text{h}$ is somewhat larger compared to the other times. This indicates limitations

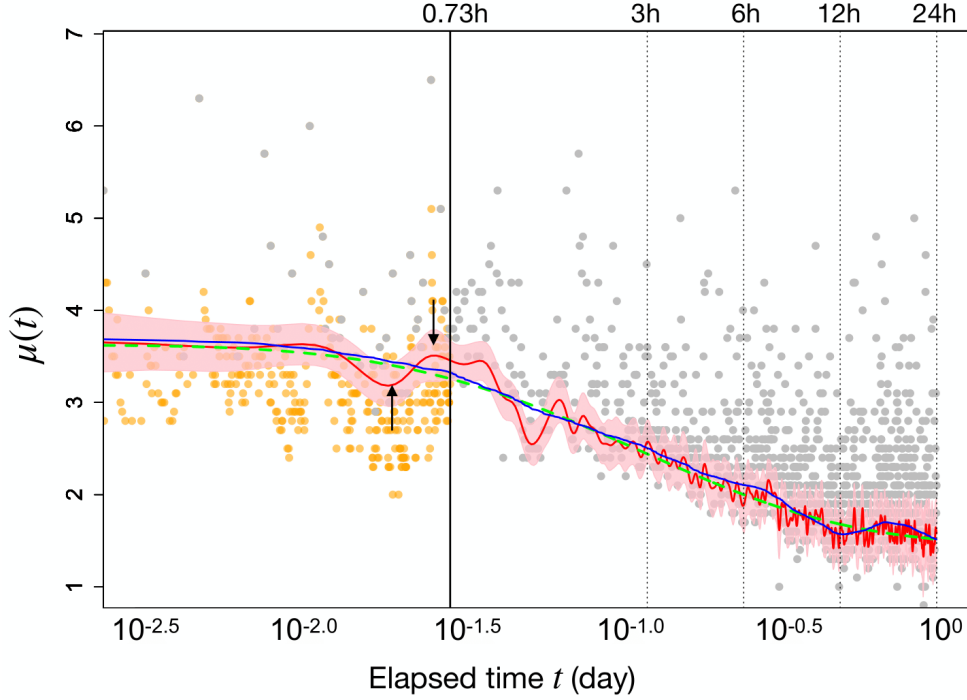


Figure 8. Visually detected aftershocks before $t \leq 0.73\text{h}$ (orange dots) proposed by Enescu et al. (2007) are added to Figure 7(d). Two arrows indicate the differences between $\mu(t)$ estimated by the proposed method and the method of Omi et al. (2014). See the caption of Figure 7 for detailed explanations.

of the Omori-Utsu law, and it would be better to apply more realistic and complex models, such as the ETAS model (Ogata 1988), for the distribution of elapsed times of the aftershocks.

Here, we conduct an additional numerical check to show that the estimated $\mu(\cdot)$ has not been affected by overfitting. Let the estimated hyperparameters for ϕ_1 and ϕ_2 be $\hat{\phi}_1 = 0.027$ and $\hat{\phi}_2 = 0.004$, respectively. The radial basis kernel function (eq. 1) indicates that small ϕ_1 and large ϕ_2 lead to a smoothed $\mu(\cdot)$ function. We re-estimate b and τ with three additional cases with fixed (ϕ_1, ϕ_2) : $(\hat{\phi}_1/3, \hat{\phi}_2)$, $(\hat{\phi}_1, 3\hat{\phi}_2)$, and $(\hat{\phi}_1/3, 3\hat{\phi}_2)$. Figure 10 shows predictive distributions of $\mu(\cdot)$ with the estimated hyperparameters (Figure 10a) and the three different cases (Figures 10b-d). The estimated $\mu(\cdot)$ oscillates the most in Figure 10(a) and the least in Figure 10(d). The most notable point in Figure 10 is that the negative peak at $t = 0.47\text{h}$ is robustly extracted regardless of the fluctuations in the hyperparameters ϕ_1 and ϕ_2 . This result is considered to indicate that the proposed method properly extracts the temporal variation in $\mu(\cdot)$, without being affected by overfitting.

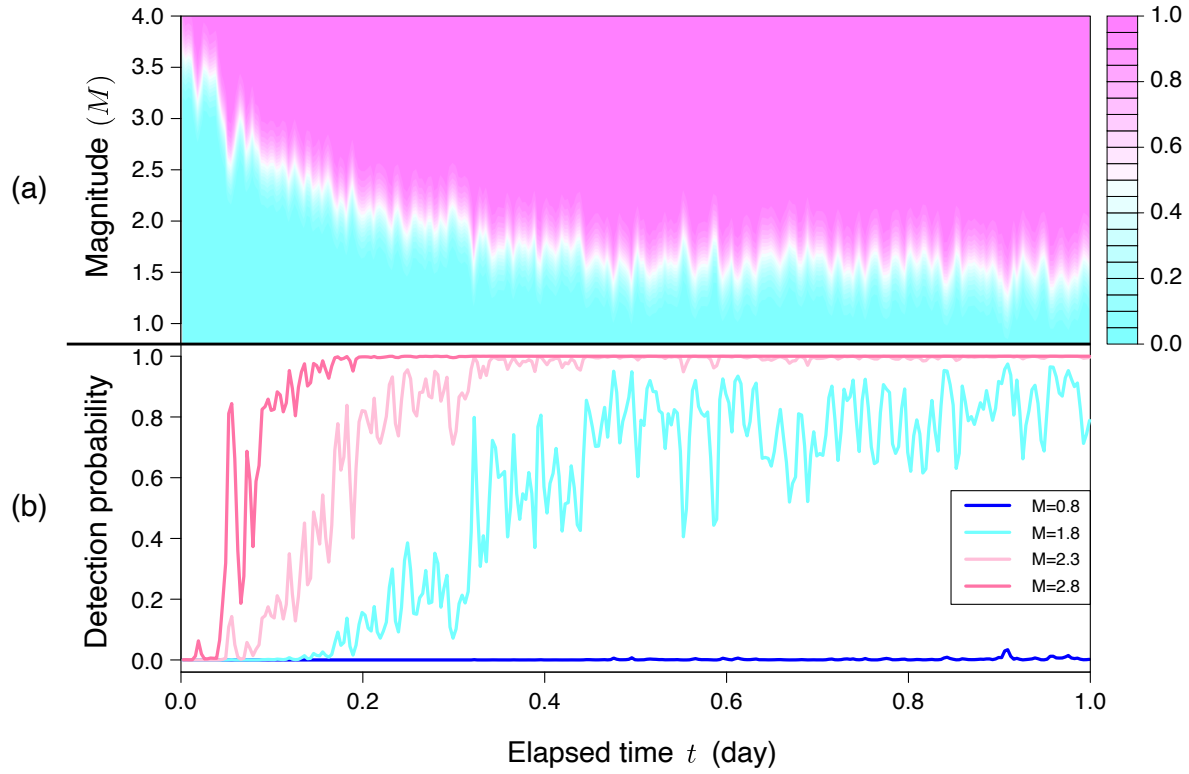


Figure 9. Estimated predictive distribution of detection function $\pi^*(M_1^*, t_1^*)$ with the application of the proposed method to the catalog data related to the 2004 Chuetsu earthquake: (a) predictive distribution of detection probability; (b) cross-sections of the predictive distribution of detection probability at the magnitudes $M = 0.8, 1.8, 2.3, 2.8$.

Table 3. Estimated posterior means and standard errors of b and $\boldsymbol{\tau} = (K, p, c)^\top$ in the case of the 2004 Chuetsu earthquake.

| Elapsed time | $t \leq 3\text{h}$ | $t \leq 6\text{h}$ | $t \leq 12\text{h}$ | $t \leq 24\text{h}$ |
|--------------|---------------------------|---------------------------|---------------------------|---------------------------|
| # of data | 192 | 355 | 655 | 1099 |
| b | 0.836 (± 0.056) | 0.741 (± 0.044) | 0.809 (± 0.035) | 0.791 (± 0.028) |
| $\ln K$ | -5.388 (± 0.262) | -4.086 (± 0.173) | -4.311 (± 0.093) | -3.230 (± 0.049) |
| p | 1.150 (± 0.110) | 1.201 (± 0.097) | 1.342 (± 0.073) | 1.228 (± 0.049) |
| $\ln c$ | -4.671 (± 0.481) | -4.358 (± 0.415) | -4.304 (± 0.341) | -4.498 (± 0.345) |

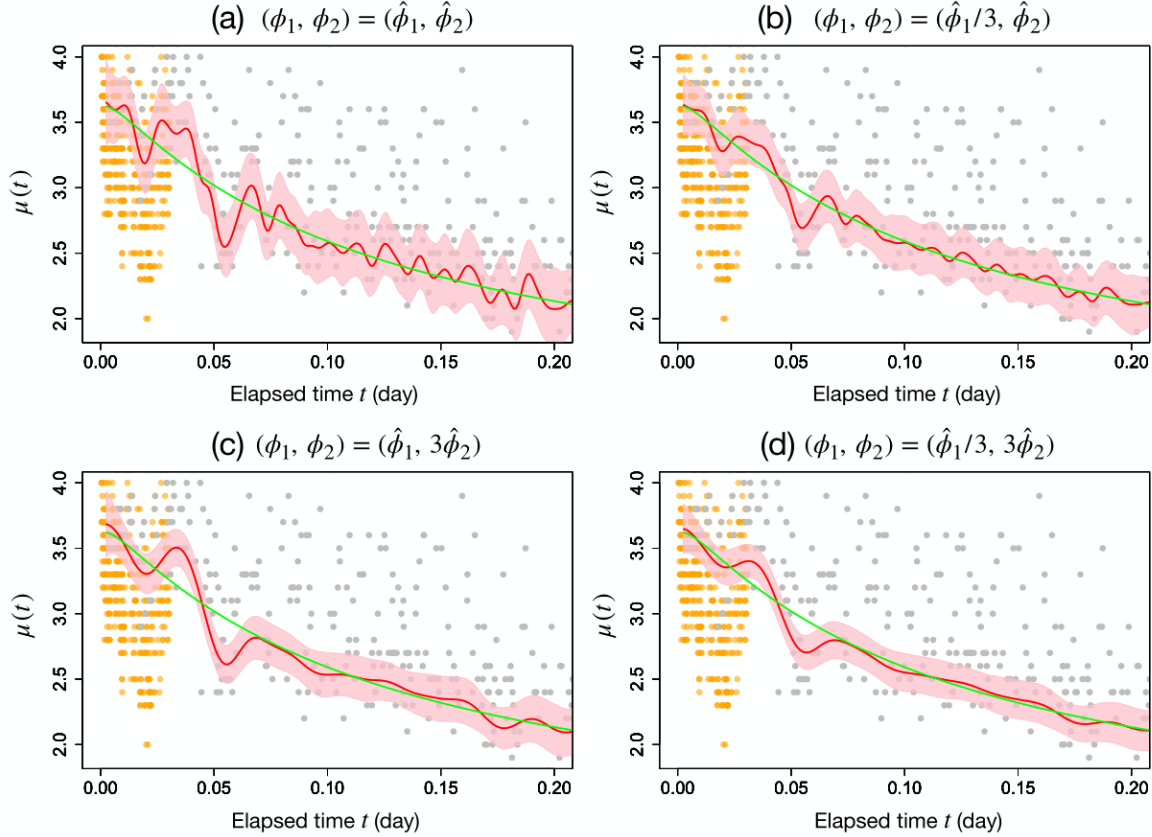


Figure 10. Predictive distribution of $\mu(\cdot)$ with different (ϕ_1, ϕ_2) : (a) $(\hat{\phi}_1, \hat{\phi}_2)$; (b) $(\hat{\phi}_1/3, \hat{\phi}_2)$; (c) $(\hat{\phi}_1, 3\hat{\phi}_2)$; (d) $(\hat{\phi}_1/3, 3\hat{\phi}_2)$, where $(\hat{\phi}_1, \hat{\phi}_2)$ is the estimated hyperparameters.

5 CONCLUDING REMARKS

Immediate prediction of seismic activities after the main shock is important to assess hazards of subsequent aftershocks. Contaminations of arriving seismic waves right after the main shock interfere with counting the number of aftershocks correctly, so that the number of detected aftershocks is underestimated. This underestimated count causes distorted estimates for the distribution of aftershocks or seismic activities. To rapidly and stably estimate the temporal changes in the occurrence rate of aftershocks with limited data right after a main shock, we introduced a GPR-based detection function to remove the effects of undetected aftershocks. Owing to the nonparametric and Bayesian properties in the GPR, the proposed detection function has four advantages superior to previous methods: (i) the resulting estimates are stable by virtue of adoption of prior information; (ii) specification of the detection function is semiparametric in the sense that $\pi(t, M; \mu, s)$ is parametric, but μ is nonparametric; (iii) MCMC sampling is effective in computing hyperparameters without computation of complicated integrations; (iv) credible intervals can be obtained in a natural way.

The limitation of the proposed method lies in the assumption on the joint intensity function (eq. 7).

It is known that real catalog data should be described by more complex intensity functions, such as represented by the ETAS model (Ogata 1988). The proposed method can be extended straightforwardly to the ETAS model, as done by Omi et al. (2014), which remains as future work.

ACKNOWLEDGMENTS

This work was supported by the Tokyo Metropolitan Resilience Project of the National Research Institute for Earth Science and Disaster Resilience (NIED), and JST CREST Grant Numbers JPMJCR1763 and JPMJCR1761. The key ideas in this study came through the activities of JSPS KAKENHI Grant-in-Aids for Early-Career Scientists No. 19K14592, 19K14671, 20K19756, Grant-in-Aids for Scientific Research (B) No. 17H01703, 17H01704, 18H03210, and Grant-in-Aid for Scientific Research (S) No. 19H05662. The travel expenses needed to discuss among co-authors was partially supported by ERI JURP 2020-A-05. One of the figures was drawn using the software Generic Mapping Tools (GMT) developed by Wessel & Smith (1998). We appreciate Prof. Aitaro Kato for constructive discussions and Prof. Bogdan Enescu for providing us his catalog related to the 2004 Chuetsu earthquake.

DATA AVAILABILITY

The official catalog of events associated with the 2004 Chuetsu earthquake is available via the website of the JMA (<http://www.data.jma.go.jp/svd/eqev/data/bulletin/>). Another catalog that also contained visually detected aftershocks (Enescu et al. 2007) was provided by Prof. Bogdan Enescu.

REFERENCES

- Aki, K., 1965. Maximum likelihood estimate of b in the formula $\log N = a - bM$ and its confidence limits, *Bull. Earthq. Res. Inst. Univ. Tokyo*, **43**, 237–239.
- de G. Matthews, A. G., Rowland, M., Hron, J., Turner, R. E., & Ghahramani, Z., 2018. Gaussian process behaviour in wide deep neural networks, *arXiv preprint: 1804.11271*.
- Enescu, B., Mori, J., & Miyazawa, M., 2007. Quantifying early aftershock activity of the 2004 mid-Niigata Prefecture earthquake (M_w 6.6), *J. Geophys. Res. Solid Earth*, **112**, 859–869.
- Genz, A. & Bretz, F., 2009. *Computation of Multivariate Normal and t Probabilities. Lecture Notes in Statistics.*, Heidelberg: Springer.
- Geweke, J. F., 1991. Efficient simulation from the multivariate normal and student- t distributions subject to linear constraints and the evaluation of constraint probabilities, *Computer Science and Statistics. Proceedings of the 23rd Symposium on the Interface.* Seattle Washington, April 21-24, 1991, 571–578.
- Geweke, J. F., 2005. *Contemporary Bayesian Econometrics and Statistics*, Wiley & Sons.

- Gutenberg, B. & Richter, C. F., 1944. Frequency of earthquakes in California, *Bull. Seism. Soc. Am.*, **34**, 185–188.
- Hainzl, S., 2016. Rate-dependent incompleteness of earthquake catalogs, *Seismol. Res. Lett.*, **87**, 337–344.
- Kagan, Y. Y. & Jackson, D. D., 2000. Probabilistic forecasting of earthquakes, *Geophys. J. Int.*, **143**, 438–453.
- Kijko, A. & Smit, A., 2017. Estimation of the frequency-magnitude gutenberg-richter *b*-value without making assumptions on levels of completeness, *Seismol. Res. Lett.*, **88**, 311–318.
- Kuwatani, T., Nagao, H., Ito, S., Okamoto, A., Yoshida, K., & Okudaira, T., 2018. Recovering the past history of natural recording media by Bayesian inversion, *Phys. Rev. E*, **98**, 043311.
- Martinsson, J. & Jonsson, A., 2018. A new model for the distribution of observable earthquake magnitudes and applications to *b*-value estimation, *IEEE Geosci. Rem. Sens. Lett.*, **15**, 833–837.
- Metropolis, N., Rosenbluth, A. W., Rosenbluth, M. N., & Teller, E., 1953. Equations of state calculations by fast computing machine, *J. Chem. Phys.*, **21**, 1087–1091.
- Mignan, A., 2012. Functional shape of the earthquake frequency-magnitude distribution and completeness magnitude, *J. Geophys. Res. Solid Earth*, **117**, B08302.
- Mignan, A., 2019. Generalized earthquake frequency–magnitude distribution described by asymmetric laplace mixture modelling, *Geophys. J. Int.*, **219**, 1348–1364.
- Ogata, Y., 1983. Estimation of the parameters in the modified omori formula for aftershock frequencies by the maximum likelihood procedure, *J. Phys. Earth*, **31**, 115–124.
- Ogata, Y., 1988. Statistical models for earthquake occurrences and residual analysis for point processes, *J. Amer. Statist. Assoc.*, **83**, 29–39.
- Ogata, Y. & Katsura, K., 1993. Analysis of temporal and spatial heterogeneity of magnitude frequency distribution inferred from earthquake catalogs, *Geophys. J. Int.*, **113**, 727–738.
- Ogata, Y. & Katsura, K., 2006. Immediate and updated forecasting of aftershock hazard, *Geophys. Res. Lett.*, **33**, L10305.
- Omi, T., Ogata, Y., Hirata, Y., & Aihara, K., 2013. Forecasting large aftershocks within one day after the main shock, *Sci. Rep.*, **3**, 2218.
- Omi, T., Ogata, Y., Hirata, Y., & Aihara, K., 2014. Estimating the ETAS model from an early aftershock sequence, *Geophys. Res. Lett.*, **41**, 850–857.
- Omi, T., Ogata, Y., Hirata, Y., & Aihara, K., 2015a. Intermediate-term forecasting of aftershocks from an early aftershock sequence: Bayesian and ensemble forecasting approaches, *J. Geophys. Res. Solid Earth*, **120**, 2561–2578.
- Omi, T., Ogata, Y., Shiomi, K., Enescu, B., Sawazaki, K., & Aihara, K., 2015b. Automatic aftershock forecasting: A test using real-time seismicity data in Japan, *Bull. Seismol. Soc. Am.*, **106**, 2450–2458.
- Omori, F., 1894. On the aftershocks of earthquake, *J. Coll. Sci. Imp. Univ. Tokyo*, **7**, 111–200.
- Petersen, K. B. & Petersen, M. S., 2012. The matrix cookbook, Technical report, Technical University of Denmark, 2007. URL <http://www2.imm.dtu.dk/pubdb/p.php?3274>.
- Qin, J., 2017. *Biased Sampling, Over-identified Parameter Problems and Beyond*, Singapore: Springer.

- Rasmussen, C. E., Williams, C. K. I., & Christopher, K. I., 2006. *Gaussian Processes for Machine Learning*, The MIT Press.
- Resenberg, P. A. & Jones, L. M., 1989. Earthquake hazard after a mainshock in California, *Science*, **243**, 1173–1176.
- Resenberg, P. A. & Jones, L. M., 1994. Earthquake aftershocks: Update, *Science*, **265**, 1251–1252.
- Ringdal, F., 1975. On the estimation of seismic detection thresholds, *Bull. Seism. Soc. Am.*, **65**, 1631–1642.
- Tanner, M. A. & Wong, W. H., 1987. The calculation of posterior distributions by data augmentation, *J. Am. Stat. Assoc.*, **82**, 528–540.
- Utsu, T., 1961. A statistical study on the occurrence of aftershocks, *J. Coll. Sci. Imp. Univ. Tokyo*, **30**, 521–605.
- Utsu, T., 1969. Aftershocks and earthquake statistics (I) — Some parameters which characterize an aftershock sequence and their interrelations —, *J. Fac. Sci., Hokkaido Univ., Ser. VII (Geophysics)*, **3**, 129–195.
- Utsu, T., 1970. Aftershocks and earthquake statistics (II) — Further investigation of aftershocks and other earthquake sequences based on a new classification of earthquake sequences —, *J. Fac. Sci. Hokkaido Univ., Ser. VII (Geophysics)*, **3**, 197–266.
- Vardi, Y., 1982. Nonparametric estimation in presence of length bias, *Ann. Stat.*, **10**, 616–620.
- Vardi, Y., 1985. Empirical distributions in selection bias models, *Ann. Stat.*, **13**, 178–203.
- Wessel, P. & Smith, W. H. F., 1998. New, improved version of generic mapping tools released, *Trans. Am. Geophys. Un.*, **79**, 579.
- Wiemer, S. & Wyss, M., 2000. Minimum magnitude of completeness in earthquake catalogs: Examples from alaska, the western united states, and japan, *Bull. Seismol. Soc. Am.*, **90**, B04310.
- Wilhelm, S. & Manjunath, B. G., 2015. *tmvtnorm: Truncated Multivariate Normal and Student t Distribution*, R package version 1.4-10.
- Zhuang, J., Ogata, Y., & Wang, T., 2017. Data completeness of the kumamoto earthquake sequence in the jma catalog and its influence on the estimation of the etas parameters, *Earth, Planets and Space*, **69**, 36.

APPENDIX A: THEORETICAL RESULTS

Lemma 1. (Formula of sum of two squared forms (Petersen & Petersen 2012, section 8.1.7)).

For any vectors \mathbf{m}_1 and \mathbf{m}_2 , and nonsingular matrices Σ_1 and Σ_2 , it holds that

$$\begin{aligned}
 & -\frac{1}{2}(\mathbf{x} - \mathbf{m}_1)^\top \Sigma_1^{-1}(\mathbf{x} - \mathbf{m}_1) \\
 & -\frac{1}{2}(\mathbf{x} - \mathbf{m}_2)^\top \Sigma_2^{-1}(\mathbf{x} - \mathbf{m}_2) \\
 & = -\frac{1}{2}(\mathbf{x} - \mathbf{m}_c)^\top \Sigma_c^{-1}(\mathbf{x} - \mathbf{m}_c) + C,
 \end{aligned} \tag{A.1}$$

where

$$\Sigma_c^{-1} = \Sigma_1^{-1} + \Sigma_2^{-1} \quad (\text{A.2})$$

$$\mathbf{m}_c = (\Sigma_1^{-1} + \Sigma_2^{-1})^{-1}(\Sigma_1^{-1}\mathbf{m}_1 + \Sigma_2^{-1}\mathbf{m}_2) \quad (\text{A.3})$$

$$C = \frac{1}{2}\mathbf{m}_c^\top \Sigma_c^{-1} \mathbf{m}_c - \frac{1}{2}(\mathbf{m}_1^\top \Sigma_1^{-1} \mathbf{m}_1 + \mathbf{m}_2^\top \Sigma_2^{-1} \mathbf{m}_2). \quad (\text{A.4})$$

Proof of Eq. (16). Because $p(\beta)$ does not involve $\boldsymbol{\mu}$, the definition of the posterior distribution is

$$L(\boldsymbol{\theta}) = p(\beta) \int p(\mathbf{M}_1 | \boldsymbol{\mu}; \beta, s^2) p(\boldsymbol{\mu} | \boldsymbol{\mu}_{\text{prior}}, \mathcal{K}_n) d\boldsymbol{\mu}, \quad (\text{A.5})$$

where $\boldsymbol{\theta} = (\beta, s^2, \phi_2^2)^\top$, $\boldsymbol{\mu}_{\text{prior}} = (\mu_{\text{prior}}(t_{11}), \dots, \mu_{\text{prior}}(t_{1n}))^\top$ is the mean of the prior distribution, and $\mathcal{K}_n = (\mathcal{K}(t_{1i}, t_{1j}))$ is the variance of the prior distribution, which is an n by n matrix. Hereafter, we ignore $p(\beta)$ because it does not have an effect on integration. Recall that the definition of the conditional distribution of M_1 given μ is given in eq. (9). It follows from

$$\begin{aligned} & \exp(\beta\mu_i)\Phi(M_{1i}; \mu_i, s^2) \\ &= \frac{\exp(\beta\mu_i)}{\sqrt{2\pi s^2}} \int_{-\infty}^{M_{1i}} \exp\left\{-\frac{(x - \mu_i)^2}{2s^2}\right\} dx \\ &= \frac{\exp(s^2\beta^2/2)}{\sqrt{2\pi s^2}} \int_{-\infty}^{M_{1i}} \exp\left[\beta x - \frac{\{\mu_i - (x + s^2\beta)\}^2}{2s^2}\right] dx \end{aligned} \quad (\text{A.6})$$

that the conditional distribution can be rewritten as

$$\begin{aligned} & \prod_{i=1}^n p(M_{1i} | \mu_i; \beta, s^2) \\ &= \beta^n \exp\left\{-\beta \sum_{i=1}^n M_{1i} - \frac{n}{2}\beta^2 s^2\right\} \prod_{i=1}^n \exp(\beta\mu_i)\Phi(M_{1i}; \mu_i, s^2) \\ &= \frac{\beta^n \exp(-\beta \sum_{i=1}^n M_{1i})}{\sqrt{(2\pi)^n |\Sigma|}} \int_{\mathbf{x} \in \mathcal{M}} \exp(\beta \mathbf{1}^\top \mathbf{x}) \\ & \quad \times \exp\left[-\frac{1}{2}\{\boldsymbol{\mu} - (\mathbf{x} + \beta\Sigma\mathbf{1})\}^\top \Sigma^{-1} \{\boldsymbol{\mu} - (\mathbf{x} + \beta\Sigma\mathbf{1})\}\right] d\mathbf{x}, \end{aligned} \quad (\text{A.7})$$

where $\Sigma = s^2 I_n$, I_n is a n by n identity matrix, and $\mathcal{M} = \otimes_{i=1}^n \{x_i \leq M_{1i}\}$. Letting $\mathbf{m}_1 = \mathbf{x} + \beta\Sigma\mathbf{1}$,

$\mathbf{m}_2 = \boldsymbol{\mu}_{\text{prior}}$, $\Sigma_1 = \Sigma$, and $\Sigma_2 = \mathcal{K}_n$ with the formula (eq. A.1), leads to

$$\begin{aligned}
L(\boldsymbol{\theta}) &= \frac{\beta^n \exp(-\beta \sum_{i=1}^n M_{1i})}{\sqrt{(2\pi)^n |\Sigma|} \sqrt{(2\pi)^n |\mathcal{K}_n|}} \int_{\mathcal{M}} \exp(\beta \mathbf{1}^\top \mathbf{x}) \\
&\quad \times \int \exp \left\{ -\frac{1}{2} (\boldsymbol{\mu} - \mathbf{m}_1)^\top \Sigma_1^{-1} (\boldsymbol{\mu} - \mathbf{m}_1) \right\} \\
&\quad \times \exp \left\{ -\frac{1}{2} (\boldsymbol{\mu} - \mathbf{m}_2)^\top \Sigma_2^{-1} (\boldsymbol{\mu} - \mathbf{m}_2) \right\} d\boldsymbol{\mu} d\mathbf{x} \\
&= \frac{\beta^n \exp(-\beta \sum_{i=1}^n M_{1i})}{(2\pi)^n \sqrt{|\Sigma| |\mathcal{K}_n|}} \\
&\quad \times \int_{\mathcal{M}} \exp(\beta \mathbf{1}^\top \mathbf{x}) \sqrt{(2\pi)^n |\Sigma_c|} \exp(C) d\mathbf{x}
\end{aligned} \tag{A.8}$$

Next, we computed m_c , Σ_c , and C in the formula. It follows from the standard argument in linear algebra that

$$\Sigma_c = (\mathcal{K}_n^{-1} + \Sigma^{-1})^{-1} = \mathcal{K}_n \tilde{\mathcal{K}}_n^{-1} \Sigma, \tag{A.9}$$

$$\mathbf{m}_c = \Sigma_c \{ \Sigma^{-1} (\mathbf{x} + \beta \Sigma \mathbf{1}) + \mathcal{K}_n^{-1} \boldsymbol{\mu}_{\text{prior}} \}, \tag{A.10}$$

$$\begin{aligned}
C &= -\frac{1}{2} \boldsymbol{\mu}_{\text{prior}}^\top \tilde{\mathcal{K}}_n^{-1} \boldsymbol{\mu}_{\text{prior}} - \frac{1}{2} (\mathbf{x} + \beta \Sigma \mathbf{1})^\top \tilde{\mathcal{K}}_n^{-1} (\mathbf{x} + \beta \Sigma \mathbf{1}) \\
&\quad + \boldsymbol{\mu}_{\text{prior}}^\top (\mathcal{K}_n + \Sigma)^{-1} (\mathbf{x} + \beta \Sigma \mathbf{1}),
\end{aligned} \tag{A.11}$$

where $\tilde{\mathcal{K}}_n = \mathcal{K}_n + \Sigma$. Rearranging the integrand so that it becomes a quadratic form of \mathbf{x} , we have

$$\begin{aligned}
L(\boldsymbol{\theta}) &= \frac{\beta^n}{\sqrt{(2\pi)^n |\tilde{\mathcal{K}}|}} \exp \left\{ -\beta \sum_{i=1}^n (M_{1i} - \mu_{\text{prior},i}) - \frac{\beta^2}{2} \mathbf{1}^\top (\Sigma - \mathcal{K}_n) \mathbf{1} \right\} \\
&\quad \times \int_{\mathcal{M}} \exp \left\{ -\frac{1}{2} (\mathbf{x} - \tilde{\boldsymbol{\mu}})^\top \tilde{\mathcal{K}}_n^{-1} (\mathbf{x} - \tilde{\boldsymbol{\mu}}) \right\} d\mathbf{x},
\end{aligned} \tag{A.12}$$

where $\tilde{\boldsymbol{\mu}} = \boldsymbol{\mu}_{\text{prior}} + \beta \mathcal{K}_n \mathbf{1}$. This is the desired conclusion.

Proof of Eq. (18). Let t_1^* be any data point may not be in the dataset. What we need to compute is

$$\begin{aligned}
&p(\mu^* | t_1^*, \mathcal{D}) \\
&= \int p(\mu^* | t_1^*, \boldsymbol{\mu}, \mathbf{t}_1) p(\boldsymbol{\mu} | \mathbf{t}_1, \mathbf{M}_1) d\boldsymbol{\mu} \\
&= \frac{\int p(\mu^* | t_1^*, \boldsymbol{\mu}, \mathbf{t}_1) p(\mathbf{M}_1 | \boldsymbol{\mu}) p(\boldsymbol{\mu} | \mathbf{t}_1) d\boldsymbol{\mu}}{\int p(\mathbf{M}_1 | \boldsymbol{\mu}) p(\boldsymbol{\mu} | \mathbf{t}_1) d\boldsymbol{\mu}}.
\end{aligned} \tag{A.13}$$

Here, the denominator of the predictive distribution is exactly the same as the marginal likelihood,

which has already been computed. Hence, it remains to show that the numerator becomes

$$\begin{aligned} & \beta^n \exp \left\{ -\beta \sum_{i=1}^n (M_{1i} - \mu_{\text{prior},i}) - \frac{1}{2} \beta^2 \left(ns^2 - \sum_{i,j} \mathcal{K}_{i,j} \right) \right\} \\ & \times \int_{\mathcal{M}} \mathcal{N}(\mu^*; D(\mathbf{x}), \tau^2) \mathcal{N}(\mathbf{x}; \tilde{\boldsymbol{\mu}}_n, \tilde{K}_n) d\mathbf{x}. \end{aligned} \quad (\text{A.14})$$

It is computed by using the formula (eq. A.1) with respect to $\boldsymbol{\mu}$, with some tedious calculus.

Proof of Eq. (21). It follows from the result of eq. (18) that

$$\begin{aligned} & P(\delta = 1 \mid M_1^*, t_1^*, \mathcal{D}) \\ & = \int P(\delta = 1 \mid M_1^*, \mu^*, \mathcal{D}) p(\mu^* \mid t_1^*, \mathcal{D}) d\mu^* \\ & = \int_{-\infty}^{\infty} \int_{-\infty}^M \mathcal{N}(z; \mu^*, s^2) \\ & \quad \times \frac{\int_{\mathcal{M}} \mathcal{N}(\mu^*; D^*(\mathbf{x}), (\tau^*)^2) \mathcal{N}(\mathbf{x}; \tilde{\boldsymbol{\mu}}_n, \tilde{K}_n) d\mathbf{x}}{\int_{\mathcal{M}} \mathcal{N}(\mathbf{x}; \tilde{\boldsymbol{\mu}}_n, \tilde{K}_n) d\mathbf{x}} d\mu^* \\ & = \int_{-\infty}^M \frac{\int_{\mathcal{M}} \mathcal{N}(z; D^*(\mathbf{x}), s^2 + (\tau^*)^2) \mathcal{N}(\mathbf{x}; \tilde{\boldsymbol{\mu}}_n, \tilde{K}_n) d\mathbf{x}}{\int_{\mathcal{M}} \mathcal{N}(\mathbf{x}; \tilde{\boldsymbol{\mu}}_n, \tilde{K}_n) d\mathbf{x}} dz \\ & = \mathbb{E}_{\text{trunc}} \left\{ \Psi \left(\frac{M_1^* - D^*(\mathbf{X})}{\sqrt{s^2 + (\tau^*)^2}} \right) \right\}. \end{aligned} \quad (\text{A.15})$$